AD-A078 612 NATIONAL AERONAUTICS AND SPACE ADMINISTRATION HAMPTO--ETC F/G 21/2
EFFECT OF PRESSURE ON STRUCTURE AND NOX FORMATION IN CO-AIR DIF--ETC(U)
OCT 79 H G MAAHS , I M MILLER

UNCLASSIFIED NASA-L-12731 NASA-TP-1448 NL

| OF |
AD
A078612

END
DATE
FILMED
1-80
DDC

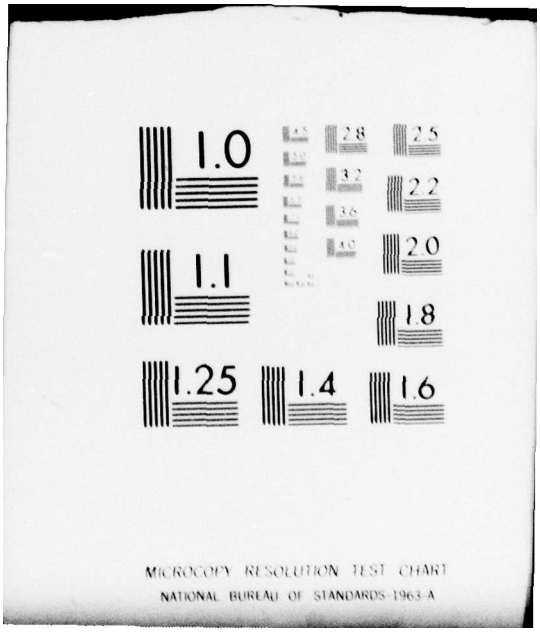
1.0
1.1
1.25
1.4
1.6
2.8
3.2
3.6
4.0
2.5
2.2
2.0
1.8
MICROCOPY RESOLUTION TEST CHART
NATIONAL BUREAU OF STANDARDS-1963-A

NASA Technical Paper 1448



# Effect of Pressure on Structure and $NO_x$ Formation in CO-Air Diffusion Flames

Howard G. Maahs and Irvin M. Miller



OCTOBER 1979





NASA

NASA Technical Paper 1448

# Effect of Pressure on Structure and $NO_X$ Formation in CO-Air Diffusion Flames

Howard G. Maahs and Irvin M. Miller
*Langley Research Center*
*Hampton, Virginia*



NASA
National Aeronautics
and Space Administration

**Scientific and Technical Information Branch**

1979

## SUMMARY

A study has been made of nitric oxide formation in a laminar CO-air diffusion flame over a pressure range from 1 to 50 atm. The carbon monoxide (CO) issued from a 3.06-mm-diameter port coaxially into a coflowing stream of air confined within a 20.5-mm-diameter chimney. Nitric oxide concentrations from the flame were measured at two carbon monoxide (fuel) flow rates: 73 standard $cm^3/min$ (sccm) and 146 sccm.

As the pressure was increased above 1 atm, the flames changed shape from wide and convex at the lowest pressures to slender and concave at 50 atm, with the most noticeable change occurring below about 10 atm. Flame height decreased as the pressure was increased from 1 atm to about 10 atm, but height was independent of pressure at higher pressures. The regimes of stable burning decreased with increasing pressure up to 50 atm, with the greatest reduction occurring between 1 and 20 atm.

The molar emission index (the moles of nitrogen oxides formed per mole of CO consumed) increased as the pressure was increased above 1 atm, reached a maximum at approximately 28 to 30 atm, and thereafter decreased slowly up to 50 atm.

Overall average rates of formation of nitrogen oxides were found to be greater than nitric oxide formation rates predicted by the conventional two-step Zeldovich mechanism when oxygen atoms are assumed to be in equilibrium with oxygen molecules, but less than those rates predicted by assuming oxygen atoms to be in dynamic steady state with the CO-air reactions. Circumstantial evidence is offered to support the proposition that the concentrations of nitrogen oxides in the flames are at their equilibrium values for pressures above about 20 atm. The case for equilibrium is not as clear at the lower pressures. It is suspected that reaction kinetics probably influence or possibly control the formation of nitrogen oxides at the lower pressures.

Comparison of the present data with data in the literature for a methane-air diffusion flame shows that for flames of comparable flame height (8 to 10 mm) and pseudoequivalence ratio (0.162), the molar emission index of a CO-air flame is significantly greater than that of a methane-air flame.


## INTRODUCTION

When fuels are burned with air, nitrogen oxides are typically formed from the interaction of nitrogen and oxygen species at the high temperatures associated with the combustion process. Some combustion devices, such as aircraft turbine engines and internal combustion engines, operate over a range of pressures rather than at one single pressure. Yet, the effect of pressure on the formation of these nitrogen oxides $NO_x$ is not well understood. Hence, there is a need to determine experimentally the possible effects of combustion pressure

on these emissions. Such information is of interest not only because of the desire to know the direction and magnitude of the effects which can be expected, but also because such information can be used as a data base for the evaluation of combustion models.

An effect of pressure on the emissions of $NO_x$ from a laminar methane-air flame has already been demonstrated in reference 1. For this flame, an increase in pressure above 1 atm is reported to cause first an increase and then a decrease in the molar emission index (the moles of $NO_x$ produced per mole of fuel consumed). The range of pressures in that investigation was from 1 to 50 atm, with the peak emission occurring at about 9 atm. A complicating uncertainty with these results, however, is that increasingly large concentrations of carbon particles formed in the flame as the pressure was increased. These carbon particles may perturb the $NO_x$-forming reactions from those which dominate when particulate carbon is not present. As one means of avoiding this complication, fuels which do not form carbon, such as carbon monoxide (CO) and hydrogen ($H_2$), could be investigated over a similar range of pressures to determine whether the observed maximum in the molar emission index is, in fact, related to the presence of carbon particles.

The present report details the results obtained from an experimental measurement of the molar emission index from a CO-air diffusion flame over the pressure range from 1 to 50 atm. As in reference 1, the diffusion flame was selected for initial study of the effect of pressure on $NO_x$ formation both because it is representative of the type of combustion encountered in many practical combustion devices (aircraft turbine engines, internal combustion engines) and because it is much easier to study safely at high pressures than are premixed flames (no tendency to flashback). This investigation was conducted in the same high-pressure facility as was used for the investigation of reference 1. A qualitative explanation of the observed results is given.

## SYMBOLS

| | |
|---|---|
| $A$ | cross-sectional area for flow within quartz shield, $cm^2$ |
| $A_b$ | projected area of base of flame, $cm^2$ |
| $A_f$ | surface area of flame, $cm^2$ |
| $C_i$ | concentration of species i, $moles/cm^3$ |
| $c_p$ | molar heat capacity, cal/mole-K |
| $d$ | thermocouple bead diameter, cm |
| $h$ | convection heat-transfer coefficient, $cal/cm^2$-sec-K |
| $I$ | emission index, (g of $NO_x$ as if all were $NO_2$)/(kg of CO consumed) |
| $I_m$ | molar emission index, (moles of $NO_x$ produced)/(mole of CO consumed) |

$I_{m,eq}$ molar emission index for $NO_X$ at equilibrium, (moles of $NO_X$ produced)/(mole of CO consumed)

$K_O$ equilibrium constant for oxygen dissociation reaction

$k_i$ reaction rate constant for ith reaction, $cm^3$/mole-sec for two-body reactions, $cm^6/mole^2$-$sec^2$ for three-body reactions (number in subscript refers to equation number)

L radiation path length, mm

$\dot{m}_i$ mass flow rate of species i, g/sec

$\dot{m}_T$ total mass flow rate in quartz shield, g/sec

n moles of species i, moles

$\dot{n}$ molar flow rate of species i, moles/sec

p pressure, atm (1 atm = 101.3 kPa)

R universal gas constant, 82.06 $cm^3$-atm/mole-K

$r_D$ diffusional rate of CO into flame zone, moles/$cm^3$-sec

$r_G$ theoretical estimate of CO consumption rate based on global rate expression (see appendix D), moles/$cm^3$-sec

$r_i$ reaction rate for formation of species i, moles/$cm^3$-sec

$r_{NO}$ rate of formation of NO by Zeldovich mechanism, moles/$cm^3$-sec

$\bar{r}^E_{CO}$ experimental average rate of consumption of CO, moles/$cm^3$-sec

$\bar{r}^E_{NO_X}$ experimental average rate of formation of $NO_X$, moles/$cm^3$-sec

$r_T$ theoretical estimate of CO consumption rate based on elementary reaction steps (see appendix D), moles/$cm^3$-sec

T temperature, K

$T_{ad}$ adiabatic flame temperature, K

$T_b$ burner temperature at exit, K

$T_c$ thermocouple temperature, K

$T_f$ flame temperature, K

$T_{I_m}$ temperature required to force agreement between $I_{m,eq}$ and $I_m$, K

$T_{ref}$ reference temperature, K

| | |
|---|---|
| $T_w$ | wall temperature within chamber, K |
| $V_{Rx}$ | reaction volume, $cm^3$ |
| $\dot{V}_{STP}$ | volumetric flow rate at standard temperature and pressure, 293 K and 1 atm, standard $cm^3$/min |
| v | velocity, cm/sec |
| $x_i$ | mole fraction of species i |
| $x_{O,eq}^{stoich}$ | equilibrium oxygen-atom mole fraction for stoichiometric premixed combustion |
| $x_{O,req}$ | oxygen-atom mole fraction required by equation (4) to give the observed $NO_x$ formation rate |
| $\Delta H_{Rx}$ | heat of combustion of CO, cal/g |
| $\epsilon$ | emissivity |
| $\lambda$ | thermal conductivity, cal/cm-K-sec |
| $\mu$ | viscosity, g/cm-sec |
| $\rho$ | density, $g/cm^3$ |
| $\sigma$ | Stefan-Boltzmann constant, $1.355 \times 10^{-12}$ cal/$cm^2$-$K^4$-sec |
| $\tau$ | residence time, msec |
| $\phi$ | equivalence ratio |
| $\phi'$ | pseudoequivalence ratio |

Subscripts:

| | |
|---|---|
| act | actual conditions |
| eff | combustion product effluent |
| f | flame conditions |
| i | ith species or ith reaction |
| in | flowing into flame zone |
| O,eq | based on assumption of oxygen atoms in equilibrium with molecular oxygen |
| O,ss | based on assumption of nonequilibrium steady-state balance for oxygen atoms in flame |

| | |
|---|---|
| o | flowing out of flame zone |
| stoich | stoichiometric conditions |

Superscript:

| | |
|---|---|
| r | reverse of reaction as written |

Chemical symbols:

| | |
|---|---|
| $CH_4$ | methane |
| CO | carbon monoxide |
| $CO_2$ | carbon dioxide |
| H | hydrogen atom |
| $H_2$ | hydrogen molecule |
| $H_2O$ | water |
| M | arbitrary third body |
| N | nitrogen atom |
| $N_2$ | nitrogen molecule |
| NO | nitric oxide |
| $NO_2$ | nitrogen dioxide |
| $NO_x$ | total nitrogen oxides (NO and $NO_2$) |
| O | oxygen atom |
| $O_2$ | oxygen molecule |
| OH | hydroxyl radical |

Abbreviations:

| | |
|---|---|
| HC | hydrocarbon |
| ppm | parts per million |
| sccm | standard $cm^3$/min |
| i.d. | inside diameter |

o.d. outside diameter

diam diameter

A bar over a symbol denotes time average.

## DESCRIPTION OF SYSTEM

The high-pressure flame system used in the present study is the same as that described in detail in reference 1. It consists of a diffusion flame burner mounted within a pressure chamber, with provisions for withdrawing combustion products and for viewing and photographing the flame. The burner is a 3.06-mm-diameter tube from which the fuel, CO, issues coaxially into a coflowing stream of air, which in turn is contained within a 20.5-mm-diameter cylindrical quartz tube concentric with the burner tube. (See fig. 1.) With a greater than stoichiometric flow rate of air, it is possible to establish on this burner arrangement a confined laminar diffusion flame, referred to as a Burke and Schumann flame (ref. 2). This is the typical overventilated diffusion flame, similar in shape to a candle flame.

To designate the overall fuel-to-air ratio, a pseudoequivalence ratio $\phi'$ is defined (in keeping with ref. 1) as the actual molar ratio of fuel to air divided by the stoichiometric molar ratio of fuel to air. The term "pseudoequivalence ratio" (rather than "equivalence ratio" only) is used to draw attention to the fact that the concept of equivalence ratio does not have the same significance for a diffusion flame as it does for a premixed flame. In an overventilated diffusion flame (i.e., $\phi' < 1$), it is generally assumed that the effective average equivalence ratio in the flame zone where reaction occurs is, in reality, very close to unity.

A schematic diagram of the high-pressure chamber, burner, and sample collection system is shown in figure 2. Ignition is accomplished by means of a resistance-heated hot-wire igniter which is retractable through a chevron packing gland at the top of the chamber. To ignite the flame, the igniter is lowered to a position 10 to 20 mm above the burner and electrical power is applied. Following ignition, the igniter is retracted out of the flow of combustion products. The combustion products exit from the top of the quartz tube (or chimney) and are swept upward into a total-sample collector by the nitrogen gas used to pressurize the system.

The diluted combustion products flow out of the system through a 5-μm particle filter and through a hot-air-heated back-pressure regulator used to maintain the chamber pressure at the desired level. At the exit of the back-pressure regulator, the sample enters a sample transfer line at near atmospheric pressure and flows to a gas analysis console. All surfaces contacted by the sample, from the chimney exit to the gas analysis console, are of stainless steel. Color photographs of the flame are taken through safety-sight glass windows located on opposite sides of the high-pressure chamber. Flow rates of CO, air, and $N_2$ are measured with calibrated linear thermal mass flowmeters having an accuracy of 1 percent of full scale. Meter ranges are 0 to 200 sccm for CO, 0 to 3000 sccm for air, and 0 to 50 000 sccm for $N_2$.

The high-pressure flame system is operated by setting the desired chamber pressure with the back-pressure regulator and pressurizing with $N_2$. After reaching pressure, flow rates for CO, air, and $N_2$ are adjusted to their target values: 73 sccm or 146 sccm for CO, the desired flow rate for air, and about 6000 sccm for $N_2$. The flame is then ignited. Two different cylinders of CO were used in the experiments: one contained 99.3 ppm $H_2$ with 327 ppm total hydrocarbon (HC) contamination; the second contained less than 10 ppm $H_2$ with less than 4 ppm HC contamination. The trace amounts of $H_2$ were intentional; their purpose was to serve as a chain carrier in initiating and sustaining the combustion of the CO. No difference was observed in the data obtained from either of these two CO cylinders. The air was zero grade, 99.995 percent pure with an HC concentration of less than 1 ppm; the $N_2$ was also 99.995 percent pure. To prevent both the appearance of a reddish-yellow luminosity near the tip of the flame and a reddish-brown deposit on the burner exit rim (apparently caused by the presence of trace amounts of iron carbonyl in the CO), the CO from the supply cylinder was first passed through a dry-ice trap and then through an adsorbent bed of Molecular Sieve 5A.

## EXPERIMENTAL MEASUREMENTS

Experimental data consist of the chemical composition of the combustion products, color photographs of the flame, and flame temperatures.

### Chemical Analyses

Chemical analyses for $CO_2$, CO, $O_2$, and $NO_x$ were performed on the total gas mixture exiting the high-pressure chamber. Analyses for CO and $CO_2$ were performed on separate (commercial) nondispersive infrared analyzers, and the analysis for $O_2$ was performed on a (commercial) paramagnetic oxygen analyzer. For the measurement of $NO_x$, a slightly modified, commercially available chemiluminescent NO-$NO_x$ analyzer was used.

Calibration gases for the infrared and paramagnetic analyzers were gas mixtures of CO, $CO_2$, and $O_2$ in $N_2$, with a stated analytical accuracy of better than ±2 percent. The calibration gases for the $NO_x$ analyzer were gas mixtures of NO in $N_2$, with a stated accuracy of ±1 percent. During an experimental run, readings of the calibration and zero gases were frequently interspersed between readings of the sample gas to eliminate possible errors caused by instrument drift.

### Photographs

Color photographs of the flame were taken with a 35-mm single-lens-reflex camera fitted with a 200-mm/f2.8 reflective lens and with color negative film. Since the intensity of the bluish color of the flame was observed to change very little with pressure, a constant camera exposure of 1/15 sec was used at all flame conditions.

### Flame Temperature

Because of the difficulty of gaining physical access to the flame and the steep thermal gradients in the flame, probing with thermocouples presents severe experimental difficulties and was not attempted. Optical techniques relying on incandescent carbon particles in the flame, like the one employed with the methane-air diffusion flame in reference 1, could not be used because of the absence of such particles. Sodium line reversal was ruled out because introduction of sodium into the flame presents certain experimental difficulties: the presence of sodium in the system could perturb the $NO_x$ formation rates and the deposition of sodium throughout the chamber and sample lines was to be avoided. These practical considerations led to the decision to settle for estimating the flame temperature at all pressures from a knowledge of the flame temperatures measured at 1 atm. To this end, the burner was removed from the high-pressure chamber and was set up on a laboratory bench at ambient pressure. Flames were established on the burner at the same flow rates of fuel and air as in the high-pressure experiments, and were probed with a chromel-alumel thermocouple with a wire diameter of 0.076 mm and a bead diameter of 0.269 mm. No attempts were made to obtain temperature profiles throughout the flames, and only peak temperatures were recorded.

## RESULTS

Experimental measurements were made at two flow rates of CO over the pressure range from 1 to 50 atm, 73 sccm and 146 sccm. The limits of stable burning and the shapes of the flames changed markedly with increasing pressure. In this section, the results of the measurements of stability and extinction limits, flame shape, $NO_x$, and flame temperature as functions of pressure are presented. The $NO_x$ data are treated in the section "Discussion."

### Stability and Extinction Limits

A rough determination of the stability and extinction limits was made with the burner prior to selecting the final experimental CO and air flow rate settings. These stability and extinction limits were determined at 1 atm, 20 atm, and 50 atm; the results are shown in figure 3. Much of the scatter in the data was caused by an air line leak which was discovered after the data had been taken; the data were then corrected to account for this leak. Hence, the indicated limits are only approximate. However, the important feature to observe in figure 3 is that the fuel-air flow rate regimes in which combustion occurs decrease considerably as pressure increases. This phenomenon is similar to that reported in reference 1 for a methane-air diffusion flame on the same burner system.

On the basis of the data in figure 3, two fuel flow rates were selected for study: 73-sccm and 146-sccm CO. Corresponding to these fuel flow rates, flow rates of air were selected at 1730 sccm and 2140 sccm, respectively, giving pseudoequivalence ratios $\Phi'$ of 0.100 and 0.162, respectively. At 73-sccm CO, the air flow rate of 1730 sccm is well within the stable region while at 146-sccm CO, the air flow rate of 2140 sccm is near the extinction boundary at

the higher pressures. A pseudoequivalence ratio $\phi'$ of 0.100 could not be easily achieved at the higher fuel flow rate of 146-sccm CO because an air flow rate of 3476 sccm would be required, a rate above the limit of the air flow meter.

## Flame Shape

Marked changes in shape and structure of the CO-air diffusion flames occur as the pressure is increased from 1 to 50 atm. These changes can be easily seen in the color photographs in figure 4. The bottom edge of each photograph is coincident with the top edge of the burner, and the lateral position of the burner is shown below each photograph. The bluish color of the flames is probably caused by $O_2$ Schumann-Runge radiation and $CO + O$ continuum radiation. (See ref. 3.)

From 1 atm to about 5 atm, the flames bow outward from the inner fuel core into the surrounding air annulus, with the result that the diameter of the flames is larger than the diameter of the burner exit. At about 10 atm, the diameter of the flames is reduced, and the shapes of the flames closely approximate cones. At pressures above 10 atm, there is an increasing concavity to the flames, and their diameters decrease noticeably. A similar behavior was observed for the methane-air diffusion flame in reference 1, wherein it was conjectured that the change in shape might result from the presence of carbon particles in the flame. In view of the present results, this conjecture is obviously incorrect, and some other explanation must be found. (It should be noted that, according to classical Burke and Schumann flame theory, no change in the size or shape of a confined laminar diffusion flame should occur as the pressure is changed.) Comparison of the shapes of the present flames with those of the methane-air flames discussed in reference 1 suggests that the only effect which can be attributed to the presence of carbon particles is a slight bulge occurring in the upper third of the methane-air flames somewhat below their tips.

The heights of the CO-air flames decrease with pressure from 1 atm to about 10 atm and thereafter remain relatively constant up to 50 atm. These flame heights are plotted in figure 5. The decrease in the height of the flame at a 146-sccm flow rate is from about $9\frac{1}{2}$ mm to about $7\frac{1}{2}$ mm, or roughly 20 percent; the decrease for the flame at a 73-sccm flow rate is from about 6 mm to about 3 mm, or roughly 50 percent.

## Oxides of Nitrogen

Results of the experimental measurements on the total oxides of nitrogen are shown in figure 6 as $I_m$, molar emission index of $NO_x$, as a function of pressure. Experimentally, this index is determined as the ratio of the measured concentrations of $NO_x$ to $CO_2$ in the effluent from the high-pressure chamber. The molar emission index is analogous to the emission index customarily used to report data on gas turbine engines; the latter is defined as the number

of grams of $NO_x$ produced, as if all nitrogen oxides were present as $NO_2$, per kilogram of fuel burned. According to these definitions, the emission index for a CO flame is 1045 times the molar emission index.

To obtain the data points in figure 6, the CO flow rates were set at their target values, three or more runs were made at different air flow rates, and concentrations of $NO_x$, CO, $CO_2$, and $O_2$ were measured. Then values of $I_m$ calculated from these data were plotted against pseudoequivalence ratio $\phi'$ and were read back at the desired values of $\phi'$ (appendix A gives the method of calculating $\phi'$). This procedure effectively eliminated the need for setting the air flow rates at precise values, a difficult task at times. It also avoids a reliance on the accuracy of the air flow meter. On the whole, over the usual ranges of $\phi'$ employed (roughly 0.08 to 0.14 for 73-sccm CO and 0.14 to 0.18 for 146-sccm CO), there was no pronounced or consistent variation of molar emission index with $\phi'$ which could be attributed to other than experimental error. Above about 30 atm, however, there did appear to be a general decrease of $I_m$ with $\phi'$, although this decrease was not large. For purposes of comparison, the molar emission index for the methane-air flame studied in reference 1 has been included in figure 6.

Figure 6 shows that for both CO flames, the molar emission index starts at a relatively low value at low pressure and increases as the pressure is increased. The molar emission index for the flame with the lower flow rate reaches a maximum of about $2.5 \times 10^{-3}$, while the $I_m$ for the flame with higher flow rate reaches a maximum of about $4.6 \times 10^{-3}$, both maxima occurring at approximately 28 to 30 atm. At still higher pressures, the $I_m$ for both flames levels off and drops slightly. These results are in contrast with those for the $CH_4$ flames, which exhibit a much smaller increase with pressure, attain an earlier maximum (at about 9 atm), and then decrease to near the low-pressure value again at 50 atm. This comparison between the $CH_4$ flame, with its low flow rate of 42 sccm, and the CO flames with a higher flow rate may at first not seem proper; however, it is noted that in terms of flame height (8 to 10 mm), pseudoequivalence ratio (0.162), and air flow rate (2450 sccm), the $CH_4$ flame is quite similar to the 146-sccm CO flame. Yet the $I_m$ for this CO flame is roughly $4\frac{1}{2}$ times the $I_m$ for the $CH_4$ flame. One obvious, at least partial, explanation is that the CO flames probably attain higher flame temperatures by virtue of their higher adiabatic flame temperatures - 2384 K for CO as compared with 2230 K for $CH_4$.[1] Furthermore, because radiation from the $CH_4$ flame is significant, its actual flame temperature is likely to be even lower than the 154 K difference in adiabatic flame temperatures would indicate. At the lower pressures, where carbon radiation from the $CH_4$ flames is not yet substantial, the $I_m$ values for both flames are in closer agreement. The effects of temperature on $I_m$ are covered in more detail in the section "Discussion."

---

[1]At 1 atm. Although there is a slight increase in adiabatic flame temperature with increase in pressure for both fuels, the increase is not dissimilar. The values of adiabatic flame temperature were calculated using the chemical equilibrium program of Svehla and McBride (ref. 4).

Only two studies could be found in the literature where measurements of $NO_x$ in CO-air flames at elevated pressures are reported. These data are compared with the present data in figure 7 on a log-log plot. The data points A, B, and C are from Haber and Coates (ref. 5) for a diffusion flame burner similar in design to the one used in the present study, but with a 1.5-mm-diameter fuel port. Most of the Haber and Coates data are not for air but for supporting atmospheres consisting of $O_2/N_2$ mixtures of varying composition. Points A, B, and C are the only data points at which direct comparisons with the present results are possible. Even though these data are for different flow rates of CO, and were obtained with a burner of smaller diameter, they are within reasonable proximity of the present data.

The data of Newitt and Lamont (ref. 6), shown as point D, are for an opposed-jet diffusion flame and represent their only data for air. Although they did not state the flow rates of their reactants, it is reasonable to assume that because of the opposed-jet flow, there must have been a turbulent, fairly well-mixed reaction zone. This type of reaction system might be expected to approach more closely that of premixed combustion rather than diffusional combustion, or, at the very least, to be somewhere between the two. However, there are other problems with the data of Newitt and Lamont that make an interpretation of their data difficult. In particular, large concentrations of unburned CO remained in the product gases even at relatively low values of $\phi'$, demonstrating that combustion was far from complete.

## Flame Temperature

As mentioned previously, temperature data were obtained for flames at both flow rates at 1 atm only. With these data and estimates of heat losses from the flames, a reasonable trend of flame temperature with increasing pressure was calculated. The raw thermocouple data were first corrected for radiation losses by the methods detailed in appendix B. Flame temperature as a function of pressure was then estimated by the procedure described in appendix C. No attempt was made to correct the thermocouple data for the heat conduction losses that can arise from the steep temperature gradients in the flame. (In severe cases, such losses could possibly produce indicated readings as much as 100 K too low, but these are extremely difficult to estimate accurately.) The resulting temperature curves are shown in figure 8 along with a plot of the adiabatic flame temperature for a CO-air flame at $\phi = 1.0$.[2] These temperature curves are believed to be fairly reasonable estimates of the true flame temperatures. For the 146-sccm CO flame, temperature increases approximately 370 K between 1 atm and 50 atm; for the 73-sccm CO flame, there is a corresponding increase of approximately 480 K. These increases compare with an increase of 140 K in adiabatic flame temperature over the same pressure range.

---

[2]It may bear repeating here that even though the overall, or pseudoequivalence ratio $\phi'$ may be considerably smaller than unity, the effective average equivalence ratio within the reaction zone must be quite close to unity. The adiabatic flame temperature was calculated from the equilibrium computer program of Svehla and McBride (ref. 4).

## DISCUSSION

In this section, the average rate of formation of $NO_X$ is estimated from the molar emission index and the average rate of consumption of CO. The question of the combustion reactions approaching equilibrium is treated, and the average rates of formation of $NO_X$ are discussed and compared with various theoretical predictions. Finally, the shapes of the molar emission index curves are discussed from the point of view of their being influenced by approach to equilibrium, particularly at the higher pressures.

### Average Rate of Formation of $NO_X$

An estimate of the average rate of formation of $NO_X$ within the flame was obtained as follows. At steady-state conditions and after complete combustion of the fuel,

$$I_m = \frac{\dot{n}_{NO_X}}{\dot{n}_{CO}}$$

where $\dot{n}_{CO}$ is the molar flow rate of CO into the flame and $\dot{n}_{NO_X}$ is the molar flow rate of $NO_X$ out of the flame. After rearrangement of this expression and division by a reaction volume $V_{Rx}$, there results

$$\frac{\dot{n}_{NO_X}}{V_{Rx}} = I_m \frac{\dot{n}_{CO}}{V_{Rx}}$$

If the reaction volume in which $NO_X$ is formed is taken to be approximately equal to (though not necessarily coincident with) the reaction volume in which CO is consumed, this expression can be rewritten as

$$\bar{r}^{-E}_{NO_X} \sim I_m \bar{r}^{-E}_{CO} \qquad (1)$$

where $\bar{r}^{-E}_{NO_X}$ is the experimental average rate of formation of $NO_X$ and $\bar{r}^{-E}_{CO}$ is the experimental average rate of consumption of CO. An estimate of the magnitude of $\bar{r}^{-E}_{CO}$ was obtained by dividing the known molar flow rate of CO $\dot{n}_{CO}$ by the volume of the flame zone, experimentally obtainable from the color photographs in figure 4. (These reaction volumes should be a fairly accurate measure of the volumes in which fuel is actually consumed since the blue zones in figure 4 are largely the result of chemiluminescence from the CO + O reaction, and since combustion was observed to be virtually complete within the flame.) Calculation of $\bar{r}^{-E}_{NO_X}$ from equation (1) implies that the reaction

volume for $NO_x$ formation is roughly equal to that for CO combustion. Although this is probably not strictly true, it is certainly reasonable to assume that these two volumes are roughly proportional. Since these reaction volumes probably do not differ by much more than a factor of 2 either way, in the absence of information to the contrary, they have been taken, for convenience, to be equal.

The photographs in figure 4 were used to determine the magnitudes of the CO reaction volumes $V_{Rx}$ by tracing the thin blue reaction zones at the surfaces of the flames and by analytically revolving the areas so defined about the center line of the flames. The resulting reaction volumes are shown in figures 9(a) and 9(b). Values for $\bar{r}_{CO}^{E}$ based on these reaction volumes are plotted as a function of pressure in figure 10(a). Also plotted in figure 10(a) are two different predictions of CO combustion rates $r_G$ and $r_T$ for a global rate expression (ref. 7) and a set of elementary reaction steps for CO combustion, respectively. Both are based on the assumption of an effective average equivalence ratio of unity in the flame zone and on initial composition. Details of the methods used for evaluating $r_G$ and $r_T$ are given in appendix D.

Because $r_G$ and $r_T$ are based on initial composition and an average $\phi$ of unity, they very likely represent the approximate maximum rates of combustion of CO in air for the present flame conditions. Departure of the experimental rates $\bar{r}_{CO}^{E}$ from these predicted rates could mean that the assumption of an average $\phi$ of unity is not a good one, that the choice of initial composition for the reactants is not appropriate, that the use of $T_f$ as an average temperature throughout the flame zone is not proper, that diffusion is really controlling the rate of reaction, or some combination of these. To treat the reaction zone in a diffusion flame in such simplified terms as these obviously oversimplifies the true situation. However, this simplified picture allows the inference from figure 10(a) (by virtue of the fact that the predicted rates are, for the most part, greater than the experimental rates) that the rates of combustion of CO in the present flames are largely diffusion controlled, certainly at pressures above 2 atm or so.

An additional reason to suspect diffusional control of the present CO-air flames, even at all pressures, is the proximity of the observed rates $\bar{r}_{CO}^{E}$ for flames at both flow rates. Because the flames have significantly different flame temperatures they also would be expected to have much different reaction rates if reaction kinetics were actually controlling. However, since these rates do not differ significantly, and since rates of diffusion are relatively insensitive to temperature, it is reasonable to infer that the combustion rates in both flames are largely diffusion controlled. A stronger argument for diffusional control can be obtained by estimating the diffusional rates of CO into the flame zone $r_D$. This estimate was carried out by the method described in appendix E, and the resulting values of $r_D$ are shown in figure 10(b). (Because these $r_D$ virtually overlay the $\bar{r}_{CO}^{E}$ in figure 10(a)

they have been plotted on a separate figure for ease in visualization.) The almost exact agreement between $\bar{r}_{CO}^{-E}$ and the estimated rates $r_D$ seems convincing evidence that the combustion reactions are, in fact, diffusion controlled. The important implication of the flames being diffusion controlled is that the combustion reactions approach equilibrium.

The average rates of formation of nitrogen oxides in the flame were estimated using equation (1) and figures 6 and 10(a) for $I_m$ and $\bar{r}_{CO}^{-E}$, respectively. The resulting rates $\bar{r}_{NO_X}^{-E}$ are plotted in figure 11. Also plotted in figure 11 are two sets of theoretical rate predictions, each based on a different set of assumptions, but both employing the conventional two-step Zeldovich mechanism for NO formation:

$$O + N_2 \rightleftharpoons NO + N \tag{2}$$

$$N + O_2 \rightleftharpoons NO + O \tag{3}$$

By standard treatments (see, for instance, ref. 1), the rate of formation of NO by the Zeldovich mechanism is given by

$$r_{NO} = 2k_2 C_O C_{N_2} \tag{4}$$

where $k_2$, the forward reaction rate constant of reaction (2), is (refs. 1, 8, and 9)

$$k_2 = 1.36 \times 10^{14}\, e^{-37947/T}$$

One set of the theoretical rate predictions in figure 11 is based on the assumption that oxygen atoms are in equilibrium with molecular oxygen, and the other is based on the assumption that there exists superequilibrium steady-state concentrations of oxygen in the flames. To obtain the theoretical rate predictions for the situation of oxygen atoms in equilibrium with molecular oxygen, the equilibrium constant (refs. 1 and 9)

$$K_O = \frac{(C_O)^2}{C_{O_2}} = 3.56 \times 10^4 \frac{1}{T} e^{-59386/T}$$

is substituted into equation (4) to eliminate the unknown oxygen-atom concentration $C_O$. In terms of mole fractions, this rate expression then becomes

$$r_{NO} = 6.90 \times 10^{13} \frac{p^{3/2}}{T^2} e^{-67640/T} x_{O_2}^{1/2} x_{N_2} \tag{5}$$

This expression was evaluated at the maximum possible values $x_{O_2} = 0.21$ and $x_{N_2} = 0.79$, at $T = T_f$, and is labeled $(r_{NO})_{O,eq}$. Rates so obtained are the maximum rates of formation of $NO_x$ attainable when oxygen atoms are in equilibrium with molecular oxygen since the effective mole fraction for oxygen in the zone where nitric oxide is formed must be substantially less than the 0.21 used, and the effective mole fraction for nitrogen is probably somewhat less than the 0.79 used. For instance, in reference 1 it was estimated that in a methane-air diffusion flame, a reasonable value for the effective oxygen mole fraction is on the order of 0.04. If this were also the case for the present CO-air diffusion flames, the predicted rates $(r_{NO})_{O,eq}$ in figure 11 would be about 0.4 times those indicated - lower yet, and farther away from agreement with the experimentally observed average rates $\bar{r}_{NO_x}^{E}$. Even though these experimentally observed rates are rough estimates, it seems unlikely that they could be in error by a factor as large as 100 or more, which they would have to be at 1 atm if the predicted rates $(r_{NO})_{O,eq}$ are correct.

One of the more reasonable explanations for the higher experimental rates is that the oxygen atoms in the flame zone are not in equilibrium with the molecular oxygen but are present in concentrations greatly in excess of equilibrium values. Such an explanation is consistent with the observation that the experimental rates approach the predicted rates $(r_{NO})_{O,eq}$ at the higher pressures where superequilibrium oxygen-atom concentrations are less likely. Calculations of the magnitude required for these superequilibrium oxygen-atom concentrations for the predicted rates to agree with $\bar{r}_{NO_x}^{E}$ can be made by substituting $\bar{r}_{NO_x}^{E}$ for $r_{NO}$ in equation (4), taking $T = T_f$ and $x_{N_2} = 0.79$, and solving for the oxygen-atom concentration. The resulting concentrations are plotted in figure 12 as the ratio $x_{O,req}/x_{O,eq}^{stoich}$, where the denominator is the equilibrium oxygen-atom mole fraction for stoichiometric premixed combustion at $T_f$. Extremely high values of the required oxygen-atom ratio occur at the lower pressures, but they decrease continually as the pressure is increased.

To obtain a more realistic estimate of the oxygen-atom concentrations, an oxygen-atom balance was made. This balance is based on the assumption that a steady-state condition exists in the flame wherein the rate of generation of oxygen atoms is exactly counterbalanced by the rate of removal of oxygen atoms. The details of this approach are given in appendix F. By this method oxygen-atom concentrations have been calculated and converted to the ratio $x_{O,ss}/x_{O,eq}^{stoich}$ and are plotted in figure 12. For the 146-sccm CO flame, this concentration of oxygen atoms is considerably greater than that required to produce the experimentally observed rates, and for the 73-sccm CO flame, this concentration is greater than that required for all pressures above about 3 atm. For pressures below about 3 atm, the estimated oxygen-atom concentration is less than that required, being as much as an order of magnitude less at

1 atm. This lower value of $x_{O,ss}$ for the 73-sccm CO flame below 3 atm implies that there is an insufficient concentration of oxygen atoms generated by the combustion process below 3 atm to account for the observed rate $\overset{-E}{r}_{NO_x}$ by the Zeldovich mechanism. However, because of the size of the potential errors involved in calculating $\overset{-E}{r}_{NO_x}$, in selecting an appropriate value for $x_{N_2}$, in making the steady-state analysis for $x_{O,ss}$, as well as in estimating $T_f$, there is insufficient cause, on these grounds alone, to invalidate the Zeldovich mechanism as being the basic mechanism for the production of nitric oxide.

Rates of formation of nitric oxide based on these steady-state oxygen-atom concentrations $(r_{NO})_{O,ss}$ have been calculated using equation (4) and are compared with the experimentally observed rates $\overset{-E}{r}_{NO_x}$ in figure 11. For this calculation, the nitrogen concentration was taken to be $x_{N_2} = 0.556$ (i.e., that nitrogen concentration existing in a stoichiometric mixture of CO and air). These rates, $(r_{NO})_{O,ss}$, are not only considerably greater than the rates predicted on the basis of oxygen-atom equilibrium but are also greater than the experimentally observed rates except for the 73-sccm CO flame below about 3 atm. Clearly, the reason why $(r_{NO})_{O,ss}$ is considerably greater than $(r_{NO})_{O,eq}$ is that the oxygen-atom concentrations based on the steady-state analysis are considerably greater than those based on the equilibrium assumption. (Examination of the analysis in appendix F shows that this is the case because the reaction step with the fastest rate of production of oxygen atoms is the combustion reaction

$$CO + O_2 \rightarrow CO_2 + O$$

and not the dissociation reaction

$$O_2 + M \rightarrow 2O + M$$

which it would have to be for atomic oxygen to be in equilibrium with molecular oxygen.)

From figure 11, it is apparent that if the Zeldovich mechanism is the correct mechanism for nitric oxide formation in CO-air diffusion flames, and if the experimentally determined rates $\overset{-E}{r}_{NO_x}$ are approximately correct, then the true average oxygen-atom concentrations in the flames are not as large as those calculated on the basis of the steady-state analysis, that is, on the basis of purely kinetic considerations. This is certainly the case at pressures above about 15 atm or so, where $(r_{NO})_{O,ss}$ is sufficiently greater than $\overset{-E}{r}_{NO_x}$ so that it is unlikely that the difference can be attributed to experimental

error. Below 15 atm, and particularly below about 3 or 4 atm, the case is not so clear. Precisely the same conclusion can be reached by inspection of figure 12, where $x_{O,req}/x_{O,eq}^{stoich}$ is less than $x_{O,ss}/x_{O,eq}^{stoich}$ at all except the lower pressures. This result leads one to consider the possibility that perhaps reaction kinetics may not be controlling the rate of formation of nitric oxide, but that diffusion might be playing a role. If diffusion were, in fact, controlling, then it necessarily follows that the $NO_x$ concentrations in the flames should approach their equilibrium values. This eventuality is considered in the following section.

## Molar Emission Index

Equilibrium values of the molar emission index calculated for stoichiometric combustion and $T = T_f$ are plotted in figure 13 as $I_{m,eq}$ along with the curves of $I_m$ from figure 6. The similarity in shape between these curves is obvious. However, $I_{m,eq}$ rises faster and peaks sooner than does $I_m$. Above about 28 atm, the curves of $I_{m,eq}$ parallel those of $I_m$ fairly well but are roughly 20 to 25 percent lower. Yet, the general similarity in shape suggests the possibility that the $NO_x$ concentrations in the flames might be approaching their equilibrium values, particularly at the higher pressures where the curves of $I_m$ and $I_{m,eq}$ are reasonably parallel, and where the required oxygen-atom ratios $x_{O,req}/x_{O,eq}^{stoich}$ in figure 12 are decreasing to lower, not so excessive values. At pressures above 28 atm, separate calculations indicate that an increase in $T_f$ of only about 50 K for both flames would be required to bring $I_{m,eq}$ into exact agreement with $I_m$, a variation certainly well within the error of estimating $T_f$. Circumstantial evidence of a similar nature (i.e., the agreement of $I_{m,eq}$ and $I_m$) was offered in reference 1 for a $CH_4$-air diffusion flame in support of the proposition that the $NO_x$ concentrations in that flame had approached equilibrium levels at pressures above about 20 atm or so. Unlike the present CO-air flames, however, it was clear for the $CH_4$-air flame that equilibrium levels of $NO_x$ had not been approached at the lower pressures, and that kinetics were still controlling. For the present CO-air flames the case is not so clear. However, because of the very large values of $x_{O,req}/x_{O,eq}^{stoich}$ at the lower pressures (see fig. 12), it is suspected that kinetics are controlling even though $I_{m,eq}$ is reasonably close to $I_m$.

Because the experimentally estimated temperatures $T_f$ are approximate in nature and because equilibrium levels of nitric oxide are quite sensitive to temperature, additional calculations were made to determine those temperatures which would have had to exist in the flames in order for $I_{m,eq}$ to coincide identically with $I_m$ over the entire range of pressures. These temperatures are plotted in figure 14 as $T_{I_m}$. Comparison of these temperatures with $T_f$ shows the average deviation between them to be about 40 K, a value well within the experimental error of the estimated temperatures $T_f$. Such close agreement between $T_{I_m}$ and $T_f$ is, nevertheless, circumstantial and therefore insufficient to prove that the $NO_x$ concentrations approach their equilibrium values at

all pressures. Further, because of the uncertain nature of $T_f$ and the great sensitivity of $I_{m,eq}$ to $T_f$, the case for or against equilibrium $NO_x$ cannot be resolved simply by consideration of the molar emission index. At the lower pressures, the very large values of $x_{O,req}/x_{O,eq}^{stoich}$ tend to argue against equilibrium there. Yet, the possibility that $NO_x$ concentrations approach equilibrium within the flames at the higher pressures above about 20 atm seems distinctly real.

To rule out the possibility that the shape of the $I_m$ curves might be caused by changes in residence time, residence times were calculated from the expression

$$\tau = \frac{V_{Rx}}{\dot{V}_{\phi=1}}$$

where $V_{Rx}$ is the reaction volume (plotted in figs. 9(a) and 9(b)) and $\dot{V}_{\phi=1}$ is the volumetric flow rate of CO and air at an average equivalence ratio of unity and at $T = T_f$. Resulting values of $\tau$ are shown in figure 15, where $\tau$ first decreases, then passes through a minimum between 5 and 7 atm, and thereafter continues to increase with increasing pressure. Since this trend is contrary to the one for $I_m$, it is obvious that the shape of the $I_m$ curves is not determined by residence-time considerations; in particular, the decrease in $I_m$ observed at the higher pressures is not caused by a corresponding decrease in $\tau$.

To help resolve this question of the $NO_x$-forming reactions approaching equilibrium, a mathematical model of a CO-air diffusion flame would be extremely useful. If such a model employed reasonable kinetic mechanisms describing combustion, and if the model adequately predicted the observed changes in flame structure with pressure, then there would be some hope that the basic details of the $NO_x$ formation processes could also be adequately modeled, and, hence, better understood. Recently, a variety of analytical approaches and computer codes capable of mathematically modeling both the complicated fluid dynamic and chemical aspects of diffusion flames have become available (refs. 10 to 19), and these could possibly prove useful.

As a final comment, it was speculated in reference 1 that among the various factors which could possibly account for the presence of the maximum in $I_m$ for a $CH_4$-air diffusion flame is the large amount of carbon in the flame. The present results clearly show that the presence of carbon in the flame is not a requirement for such a maximum. Although such carbon could still conceivably affect the location of the maximum, it is obviously not necessary for such a maximum to exist. Based on the present data and analysis, the preferred explanation for the shape of the $I_m$ curves as a function of pressure for both the CO-air and $CH_4$-air diffusion flames is that equilibrium levels of $NO_x$ are approached in the flames at the higher pressures.

## CONCLUDING REMARKS

A study has been made of nitric oxide formation in a laminar CO-air diffusion flame over a range of pressures from 1 to 50 atm. The carbon monoxide (fuel) issued from a 3.06-mm-diameter port coaxially into a coflowing stream of air confined within a 20.5-mm-diameter chimney. Experimental measurements of nitric oxide concentrations were made at two carbon monoxide (fuel) flow rates: 73 standard $cm^3$/min (sccm) and 146 sccm. The flow rates were held constant over the entire range of pressures from 1 to 50 atm. The stability and extinction limits, flame shape, flame height, $NO_x$, and flame temperature were all affected by changes in pressure. Based on these experimental data and their analysis, the following observations and conclusions are offered:

1. The shape of CO-air diffusion flames changes from wide and convex at 1 atm to slender and concave at 50 atm. The most noticeable change in shape occurs below about 10 atm.

2. The height of the flames decreases with pressure from 1 atm to about 10 atm or so, and thereafter remains relatively constant up to 50 atm. For the flame with 146-sccm flow rate, the decrease is from about $9\frac{1}{2}$ mm to about $7\frac{1}{2}$ mm; for the 73-sccm flame, the decrease is from about 6 mm to a little over 3 mm.

3. The regimes of stable burning decrease as the pressure is increased, with the greatest reduction occurring between 1 atm and 20 atm.

4. The concentrations of nitrogen oxides produced by the flames were measured and reported as molar emission index (the moles of nitrogen oxides formed per mole of carbon monoxide consumed). For both flames, the molar emission index increases as the pressure is increased above 1 atm, reaches a maximum in the neighborhood of 28 to 30 atm, and thereafter decreases slowly up to 50 atm. Hence, at all pressures above 1 atm and up to at least 50 atm, the molar emission index is greater than that at 1 atm.

5. Comparison of the present data with data in the literature for a methane-air diffusion flame shows that for flames of comparable flame height (8 to 10 mm) and pseudoequivalence ratio (0.162), the molar emission index of a CO-air flame can be as much as $4\frac{1}{2}$ times that of a methane-air flame.

6. Those few data in the literature on nitric oxide concentrations generated by coaxial CO-air diffusion flames are in reasonable agreement with the present data.

7. Overall average reaction rates of carbon monoxide were determined for the diffusion flames. Comparison of these rates with kinetic predictions and diffusion rates suggests that the carbon monoxide combustion reactions are diffusion controlled. The implication of this is that these combustion reactions approach equilibrium.

8. Overall average rates of formation of nitrogen oxides were estimated from the data. These rates are greater than nitric oxide formation rates predicted by the conventional two-step Zeldovich mechanism when oxygen atoms are assumed to be in equilibrium with oxygen molecules, but are, in general, less than the predicted rates when oxygen atoms are assumed to be in dynamic steady state with the CO-air reactions.

9. Circumstantial evidence is offered in support of the proposition that the concentrations of nitrogen oxides in the CO-air flames are near their equilibrium values for pressures above about 20 atm. The case for equilibrium is not clear at the lower pressures, but it is suspected that kinetics probably influence or even control the formation of nitrogen oxides at the lower pressures.

Langley Research Center
National Aeronautics and Space Administration
Hampton, VA 23665
August 10, 1979

## APPENDIX A

### METHOD OF CALCULATING PSEUDOEQUIVALENCE RATIO

The pseudoequivalence ratio $\phi'$ was obtained from the composition of the effluent from the high-pressure chamber. It was calculated from its definition

$$\phi' \equiv \frac{(n_{CO}/n_{O_2})_{act}}{(n_{CO}/n_{O_2})_{stoich}} = \frac{(x_{CO}/x_{O_2})_{act}}{(x_{CO}/x_{O_2})_{stoich}} \tag{A1}$$

where

$$\left(\frac{x_{CO}}{x_{O_2}}\right)_{stoich} = 2$$

The ratio of CO to $O_2$ in the numerator was obtained from an analysis of the effluents as the ratio of the unburned CO plus the burned CO ($CO_2$) to the sum of the excess oxygen remaining after combustion and the amount of oxygen consumed during the combustion, as indicated in the following equation:

$$\left(\frac{x_{CO}}{x_{O_2}}\right)_{act} = \left(\frac{x_{CO} + x_{CO_2}}{x_{O_2} + \frac{1}{2} x_{CO_2}}\right)_{eff}$$

The air flow rate was calculated from $\phi'$.

## APPENDIX B

### THERMOCOUPLE CORRECTIONS FOR RADIATION LOSSES

To correct the raw thermocouple readings for radiation losses, the following formula of Kaskan from reference 20 was used:

$$T_f - T_c = \frac{1.25\varepsilon\sigma d^{3/4}}{\lambda}\left(\frac{\mu}{\rho v}\right)^{1/4}(T_c^4 - T_w^4)$$

The value of $\varepsilon$ was taken to be 0.25 (refs. 21 and 22), $d$ was obtained from micrometer measurement of the thermocouple bead, the product $\rho v$ was obtained from the expression $\rho v = \dot{m}_T/A$, and $\lambda$ and $\mu$ were evaluated at $T_f$ for a $CO_2$ and $N_2$ mixture resulting from the stoichiometric combustion of CO and air. Mixture properties for $\mu$ and $\lambda$ were calculated using Wilke's equation (ref. 23) and Brokaw's equation (ref. 23), respectively. The pure-gas properties for $\mu$ and $\lambda$ were obtained from reference 24. The quantity $T_w^4$ was considered negligible compared with $T_c^4$, and was therefore dropped from the equation.

## APPENDIX C

### ESTIMATION OF FLAME TEMPERATURE AS A FUNCTION OF PRESSURE

An approximate estimate of flame temperature was obtained by mathematically accounting for those sources of heat loss from the flame which reduce its temperature to some value below the adiabatic flame temperature, as follows.

When there is no heat loss from the flame,

$$\begin{matrix}\text{Heat} \\ \text{generated}\end{matrix} + \begin{matrix}\text{Sensible} \\ \text{heat in}\end{matrix} = \begin{matrix}\text{Sensible} \\ \text{heat out}\end{matrix}$$

where the heat generated is from the heat of combustion and the sensible heat refers to the heat content of the gases flowing into the flame zone (CO and air) and out of the flame zone ($CO_2$ and $N_2$). Stated mathematically, this becomes

$$\Delta H_{Rx}\dot{m}_{CO} + \sum c_{p,in}\dot{n}_i(T_{in} - T_{ref}) = \sum c_{p,o}\dot{n}_o(T_{ad} - T_{ref}) \qquad (C^1)$$

When there is heat loss from the flame,

$$\begin{matrix}\text{Heat} \\ \text{generated}\end{matrix} + \begin{matrix}\text{Sensible} \\ \text{heat in}\end{matrix} = \begin{matrix}\text{Sensible} \\ \text{heat out}\end{matrix} + \begin{matrix}\text{Heat radiated} \\ \text{to chamber}\end{matrix} + \begin{matrix}\text{Heat radiated} \\ \text{to burner}\end{matrix} + \begin{matrix}\text{Heat convected} \\ \text{to burner}\end{matrix}$$

or

$$\Delta H_{Rx}\dot{m}_{CO} + \sum c_{p,in}\dot{n}_{in}(T_{in} - T_{ref}) = \sum c_{p,o}\dot{n}_o(T_f - T_{ref}) + A_f\varepsilon_f\sigma(T_f^4 - T_w^4) + A_b\varepsilon_f\sigma(T_f^4 - T_b^4) + hA_b(T_f - T_b) \qquad (C2)$$

Equating equations ($C^1$) and (C2), collecting terms, neglecting $T_w^4$ and $T_b^4$ relative to $T_f^4$, and approximating $T_b$ by $T_{in}$, gives

$$\sum c_{p,o}\dot{n}_o(T_{ad} - T_f) = (A_f + A_b)\varepsilon_f\sigma T_f^4 + hA_b(T_f - T_{in}) \qquad (C3)$$

The term $\sum c_{p,o}\dot{n}_o$ was evaluated for a $CO_2$ and $N_2$ mixture resulting from the stoichiometric combustion of CO and air and from the known flow rate for CO. The quantities $A_f$ and $A_b$ were obtained from measurements of the external boundaries of the luminous zones in the color photographs in figure 4 and are shown plotted in figures 16 and 17. The emissivity $\varepsilon_f$ was obtained using the method of reference 25. For this purpose, the luminous zones in figure 4 were taken to consist of a $CO_2$ and $N_2$ mixture resulting from the stoichiometric combustion of CO and air, the radiation path length L was obtained from measurements of the thickness of these luminous zones in the upper part of the flames

## APPENDIX C

(L is shown plotted in fig. 18), and corrections for pressure broadening of the $CO_2$ bands were made by employing correction factors obtained from reference 25.

At 1 atm, where $T_f$ is known from direct thermocouple measurement, equation (C3) was solved for the heat-transfer coefficient h, giving 0.362 cal/cm$^2$-min-K for the 146-sccm CO flame, and 0.331 cal/cm$^2$-min-K for the 73-sccm CO flame. Because the heat-transfer coefficient is a function of the mass flow rate, the various transport properties of the gases, and the geometry of the burner, and because these are largely invariant with pressure, these calculated heat-transfer coefficients are taken to be applicable at all pressures. This procedure, then, allows the solution of equation (C3) for $T_f$ at all other pressures. The resulting temperature curves are shown plotted in figure 8. Because of the extensive calculations and necessary approximations involved in obtaining these temperature curves, they must be considered approximate; nevertheless, they are believed to represent a fairly reasonable trend of flame temperature with increasing pressure.

## APPENDIX D

## ESTIMATION OF THEORETICAL CO REACTION RATES

Howard, Williams, and Fine (ref. 7) give for the global rate of oxidation of CO to form $CO_2$, in the presence of water vapor

$$r_G = 1.3 \times 10^{14} e^{-15098/T} C_{CO} C_{O_2}^{1/2} C_{H_2O}^{1/2} \qquad (D1)$$

In a diffusion flame, combustion within the flame zone may reasonably be assumed to occur at an overall average equivalence ratio $\phi = 1$; hence, for the present CO-air flames, the initial composition can be taken to be

$$x_{CO} = 0.296$$

$$x_{O_2} = 0.148$$

$$x_{N_2} = 0.556$$

Hydrogen is almost always present in small concentrations because of virtually unavoidable contamination with water vapor, or by intentional addition. For most of the experimental runs, the CO cylinder with 99.3 ppm $H_2$ was used since no difference in results was observed between this concentration and the lower concentration of 10 ppm $H_2$ in the second cylinder. Therefore, for purposes of estimating the theoretical CO combustion rates, the concentration in the fuel gas was taken to be approximately 100 ppm or $x_{H_2} = 10^{-4}$. In a stoichiometric mixture of CO fuel and air, this gives

$$x_{H_2} = 2.96 \times 10^{-5}$$

Taking $x_{H_2O} \sim x_{H_2}$, and substituting the given values of mole fractions into equation (D1) at $T = T_f$, the rate curves labeled $r_G$ in figure 10(a) are obtained.

Several other expressions for the global rate of oxidation of CO also appear in the literature. (See, for instance, refs. 26 to 29.) For the same flame conditions, these expressions predict rates from as much as $6\frac{1}{2}$ times the $r_G$ values in figure 10(a) to as low as 1/5 these values, and some have somewhat

different temperature dependencies. The rate expression of Howard, Williams, and Fine (ref. 7) was selected here because it is more recent and because it is based on more extensive data. In addition, it predicts rates which are reasonable averages of those predicted by the other rate expressions.

An alternate estimate of the rate of combustion of CO can be obtained from the elementary reaction steps

$$CO + OH \rightarrow CO_2 + H \qquad (D2)$$

$$CO + O_2 \rightarrow CO_2 + O \qquad (D3)$$

$$CO + O + M \rightarrow CO_2 + M \qquad (D4)$$

The reaction rate constants $k_i$ associated with these reactions are (ref. 8)

$$k_2 = 4 \times 10^{12} e^{-4026/T}$$

$$k_3 = 1.6 \times 10^{13} e^{-20634/T}$$

$$k_4 = 6 \times 10^{13}$$

with consistent units in moles, $cm^3$, and sec. Reaction rates $r_2$, $r_3$, and $r_4$ associated with reactions (D2) to (D4) were evaluated for both the 146-sccm CO flame and the 73-sccm CO flame as follows. The hydroxyl radical and oxygen-atom concentrations for use in reactions (D2) and (D4) were determined for equilibrium conditions at $T = T_f$ and for an equivalence ratio of hydrogen appropriate to the present system of 100 ppm $H_2$ in the CO fuel, $\phi_{H_2} = 10^{-4}$ (i.e., when the fuel is taken to be at an overall average $\phi$ of unity with respect to air). The results were then scaled for $x_{O_2} = 0.148$ in the flame. The rate $r_3$ was calculated using the mole fractions for CO and $O_2$ given earlier. Comparison of these calculated rates showed that $r_4 << r_3$, and $r_2$ is roughly 10 percent of $r_3$ for the 146-sccm CO flame, and roughly 2 percent of $r_3$ for the 73-sccm CO flame. Hence, a rough estimate of the theoretical reaction rates for CO can be written

$$r_T = r_2 + r_3$$

where, for the 146-sccm CO flame, $r_T \approx 1.1 r_3$, and for the 73-sccm CO flame, $r_T \approx 1.02 r_3$. These rates were calculated at $T = T_f$ and $\phi = 1$ and are plotted in figure 10(a). The close agreement between $r_T$ and $r_G$ for each of the two CO flow rates lends confidence that these rate predictions are of the proper order of magnitude.

## APPENDIX E

### ESTIMATION OF DIFFUSION RATES

To estimate the rate of diffusion of CO from the core of the flame into the reaction zone, Fick's law can be written as

$$\vec{J} = -D \frac{dC_{CO}}{d\ell}$$

where

$\vec{J}$ diffusional flux of CO

D diffusion coefficient for CO (taken as CO into $N_2$)

$\frac{dC_{CO}}{d\ell}$ concentration gradient

Expressing $C_{CO}$ in terms of $x_{CO}$ by the perfect gas law, and writing the concentration gradient in finite difference form, there results

$$\vec{J} = D \frac{p}{RT_f} \left[ \frac{(x_{CO})_{core} - (x_{CO})_{edge}}{L} \right]$$

where the subscripts "core" and "edge" refer to the inner and outer edges of the flame zone, respectively, and L is the thickness of the flame zone (the same as the radiation path length in appendix C). Taking $(x_{CO})_{core} = 1$ and $(x_{CO})_{edge} = 0$, and writing the diffusional flux as a volumetric diffusional rate $r_D$ using the thickness of the flame zone to define the diffusional volume, there is obtained

$$r_D = \frac{\vec{J}}{L} = \frac{pD}{RT_f L^2}$$

Values for D were calculated using the method of Hirschfelder as described in reference 23, and L was taken from figure 18.

## APPENDIX F

### ESTIMATION OF OXYGEN-ATOM CONCENTRATION

In the combustion system of CO and air, the primary reactions involving oxygen atoms are (see, for instance, ref. 8)

$$CO + O_2 \rightarrow CO_2 + O \tag{F1}$$

$$CO + O + M \rightarrow CO_2 + M \tag{F2}$$

$$O_2 + M \rightleftarrows 2O + M \tag{F3}$$

$$O + N_2 \rightarrow NO + N \tag{F4}$$

$$N + O_2 \rightarrow NO + O \tag{F5}$$

The reaction rate constants $k_i$, in units of moles, $cm^3$, and sec, for these reactions are given by

$$k_1 = 1.6 \times 10^{13}\, e^{-20634/T}$$

$$k_2 = 6 \times 10^{13}$$

from reference 8, and by

$$k_3 = 3.56 \times 10^{18}\, \frac{1}{T}\, e^{-59386/T}$$

$$k_3^r = 1 \times 10^{14}$$

$$k_4 = 1.36 \times 10^{14}\, e^{-37947/T}$$

$$k_5 = 6.4 \times 10^{9}\, Te^{-3145/T}$$

from reference 9, where all rate constants are for the forward reaction as written, except the rate constant designated with a superscript r, which is for the reverse reaction. Since $CO_2$ and NO are stable reaction products which exit the flame zone, only the forward rates of reactions (F1), (F2), (F4), and (F5) are considered; but since oxygen atoms are not a stable reaction product, the reverse rate of reaction (F3) is considered in addition to its forward rate. Employing a steady-state assumption for oxygen atoms in the flame, the rate of production of oxygen atoms is set equal to the rate of destruction of oxygen atoms. This equality can be expressed in terms of the rates of reactions (F1) to (F5) as

$$r_1 + 2r_3 + r_5 = r_2 + 2r_3^r + r_4 \tag{F6}$$

where all rates $r$ stand for the forward rates of the reactions as written, except the rate with the superscript $r$, which designates the reverse reaction. An order of magnitude analysis of equation (F6) for temperatures between 1600 K and 2200 K, for all pressures between 1 and 50 atm, and for mole fractions $x_{CO} = 0.296$, $x_{O_2} = 0.148$, $x_{N_2} = 0.556$, with $x_M = 1.000$, and with the assumption that atomic nitrogen is in equilibrium with molecular nitrogen, indicates that

$$r_1 >> 2r_3$$

$$r_1 >> r_5$$

$$r_2 = O(2r_3^r) \quad \text{for high oxygen-atom concentrations}$$

$$r_2 >> r_4$$

Hence, to a reasonable approximation at all temperatures and pressures in the flame,

$$r_1 \approx r_2 + 2r_3^r \tag{F7}$$

Substitution of the appropriate rate expressions into equation (F7) permits a solution for the steady-state concentration of oxygen atoms. In terms of mole fractions, this concentration is

$$x_O = -0.15x_{CO} + \left(0.0225x_{CO}^2 + 6.565 \frac{T}{p} e^{-20634/T} x_{CO}x_{O_2}\right)^{1/2} \tag{F8}$$

Taking $x_{CO} = 0.296$ and $x_{O_2} = 0.148$, this simplifies to

$$x_{O,ss} = -0.0444 + \left(1.971 \times 10^{-3} + 0.2876 \frac{T}{p} e^{-20634/T}\right)^{1/2} \tag{F9}$$

where the subscript $ss$ is appended to designate that this oxygen-atom concentration is not an experimentally determined value, but is instead an estimated value derived from the present steady-state analysis. It should be pointed out that since the reverse of reaction (F1) was neglected in the analysis, the values of $x_{O,ss}$ obtained from equation (F9) probably represent an upper limit for $x_O$ which might be expected in the flame. The (F2) reverse reaction, which produces oxygen atoms, was also neglected; but because this reaction is highly improbable, its contribution to the concentration of oxygen atoms is insignificant. Values of $x_{O,ss}$ evaluated from equation (F9) at the appropriate values of $T_f$ and $p$, are plotted in figure 12 as $x_{O,ss}/x_{O,eq}^{stoich}$.

## REFERENCES


1. Miller, Irvin M.; and Maahs, Howard G.: High-Pressure Flame System for Pollution Studies With Results for Methane-Air Diffusion Flames. NASA TN D-8407, 1977.

2. Burke, S. P.; and Schumann, T. E. W.: Diffusion Flames. Proceedings of the First Symposium on Combustion and the Second Symposium on Combustion, Combustion Inst., c.1965, pp. 2-11.

3. Gaydon, A. G.; and Wolfhard, H. G.: Flames. Their Structure, Radiation and Temperature. Third ed., Rev. Chapman & Hall Ltd. (London), 1970.

4. Svehla, Roger A.; and McBride, Bonnie J.: FORTRAN IV Computer Program for Calculation of Thermodynamic and Transport Properties of Complex Chemical Systems. NASA TN D-7056, 1973.

5. Haber, F.; and Coates, J. E.: Über die Stickoxydbildung bei der Kohlenoxydverbrennung. Z. Phys. Chem., Bd. LXIX, 1909, pp. 337-388.

6. Newitt, Dudley M.; and Lamont, Frank G.: Gaseous Combination at High Pressures, Part XVI: - Nitric Oxide Formation in Continuous High-Pressure Flames of Carbonic Oxide in Oxygen-Nitrogen Atmospheres. Proc. Roy. Soc. London, ser. A, vol. CXXXIX, no. A 837, Jan. 2, 1933, pp. 83-93.

7. Howard, J. B.; Williams, G. C.; and Fine, D. H.: Kinetics of Carbon Monoxide Oxidation in Postflame Gases. Fourteenth Symposium (International) on Combustion, Combustion Inst., 1973, pp. 975-986.

8. Jachimowski, Casimir J.: Analytical Study of Mechanisms for Nitric Oxide Formation During Combustion of Methane in a Jet-Stirred Combustor. NASA TN D-8098, 1975.

9. Bracco, Frediano V.: Nitric Oxide Formation in Droplet Diffusion Flames. Fourteenth Symposium (International) on Combustion, Combustion Inst., 1973, pp. 831-842.

10. Jones, Walter W.; and Boris, Jay P.: Flame and Reactive Jet Studies Using a Self-Consistent Two-Dimensional Hydrocode. J. Phys. Chem., vol. 81, no. 25, Dec. 15, 1977, pp. 2532-2534.

11. Markatos, N. C.; Spalding, D. B.; and Srivatsa, S. K.: Prediction of the Hydrodynamics and Chemistry of Methane-Air Flames in a Two Concentric Tube Combustor. NASA CR-135412, 1978.

12. Lockwood, F. C.: The Modelling of Turbulent Premixed and Diffusion Combustion in the Computation of Engineering Flows. Combust. & Flame, vol. 29, no. 2, 1977, pp. 111-122.

13. Pratt, David T.: Calculation of Chemically Reacting Flows With Complex Chemistry. Volume 2 of Studies in Convection, B. E. Launder, ed., Academic Press, Inc., 1977, pp. 191-220.

14. Miller, James A.; and Kee, R. J.: Chemical Nonequilibrium Effects in Hydrogen-Air Laminar Jet Diffusion Flames. SAND77-8505, Sandia Lab., Apr. 1977.

15. Kee, R. J.; and Miller, J. A.: A Split-Operator, Finite Difference Solution for Axisymmetric Laminar Jet Diffusion Flames. A Collection of Technical Papers - AIAA 3rd Computational Fluid Dynamics Conference, June 1977, pp. 82-94.

16. Elghobashi, S.; Spalding, D. B.; and Srivatsa, S. K.: Prediction of Hydrodynamics and Chemistry of Confined Turbulent Methane-Air Flames With Attention to Formation of Oxides of Nitrogen. NASA CR-135179, 1977.

17. Moore, J. G.; and Moore, J.: The Distributions of Temperature and Major Species in Laminar Diffusion Flames. Sixteenth Symposium (International) on Combustion, Combustion Inst., 1976, pp. 1123-1132.

18. Varma, A. K.; Beddini, R. A.; and Fishburne, E. S.: Second-Order Closure Analysis of Turbulent Reacting Flows. Proceedings of the 1976 Heat Transfer and Fluid Mechanics Institute, Allan A. McKillop, James W. Baughn, and Harry A. Dwyer, eds., Stanford Univ. Press, c.1976, pp. 229-240.

19. Mitchell, Reginald Eugene: Nitrogen Oxide Formation in Laminar Methane-Air Diffusion Flames. D. Sc. Thesis, Massachusetts Inst. Technol., 1975.

20. Fristrom, R. M.; and Westenberg, A. A.: Flame Structure. McGraw-Hill Book Co., c.1965.

21. Sarofim, A. F.; and Pohl, J. H.: Kinetics of Nitric Oxide Formation in Premixed Laminar Flames. Fourteenth Symposium (International) on Combustion, Combustion Inst., 1973, pp. 739-754.

22. Takagi, Toshimi; Ogasawara, Mitsunobu; Fujii, Kenichi; and Daizo, Masahito: A Study on Nitric Oxide Formation in Turbulent Diffusion Flames. Fifteenth Symposium (International) on Combustion, Combustion Inst., 1974, pp. 1051-1059.

23. Reid, Robert C.; and Sherwood, Thomas K.: The Properties of Gases and Liquids. McGraw-Hill Book Co., Inc., 1958.

24. Hilsenrath, Joseph; Beckett, Charles W.; Benedict, William S.; Fano, Lilla; Hoge, Harold J.; Masi, Joseph F.; Nuttall, Ralph L.; Touloukian, Yeram S.; and Woolley, Harold W.: Tables of Thermal Properties of Gases. NBS Circ. 564, U.S. Dep. Commer., Nov. 1, 1955.

25. McAdams, William H.: Heat Transmission. Third ed. McGraw-Hill Book Co., Inc., 1954.

26. Dryer, F. L.; and Glassman, I.: High-Temperature Oxidation of CO and $CH_4$. Fourteenth Symposium (International) on Combustion, Combustion Inst., 1973, pp. 987-1003.

27. Williams, G. C.; Hottel, H. C.; and Morgan, A. C.: The Combustion of Methane in a Jet-Mixed Reactor. Twelfth Symposium (International) on Combustion, Combustion Inst., 1969, pp. 913-925.

28. Hottel, H. C.; Williams, G. C.; Nerheim, N. M.; and Schneider, G. R.: Kinetic Studies in Stirred Reactors: Combustion of Carbon Monoxide and Propane. Tenth Symposium (International) on Combustion, Combustion Inst., 1965, pp. 111-121.

29. Koslov, G. I.: On High-Temperature Oxidation of Methane. Seventh Symposium (International) on Combustion, Butterworths Sci. Publ. (London), 1959, pp. 142-149.

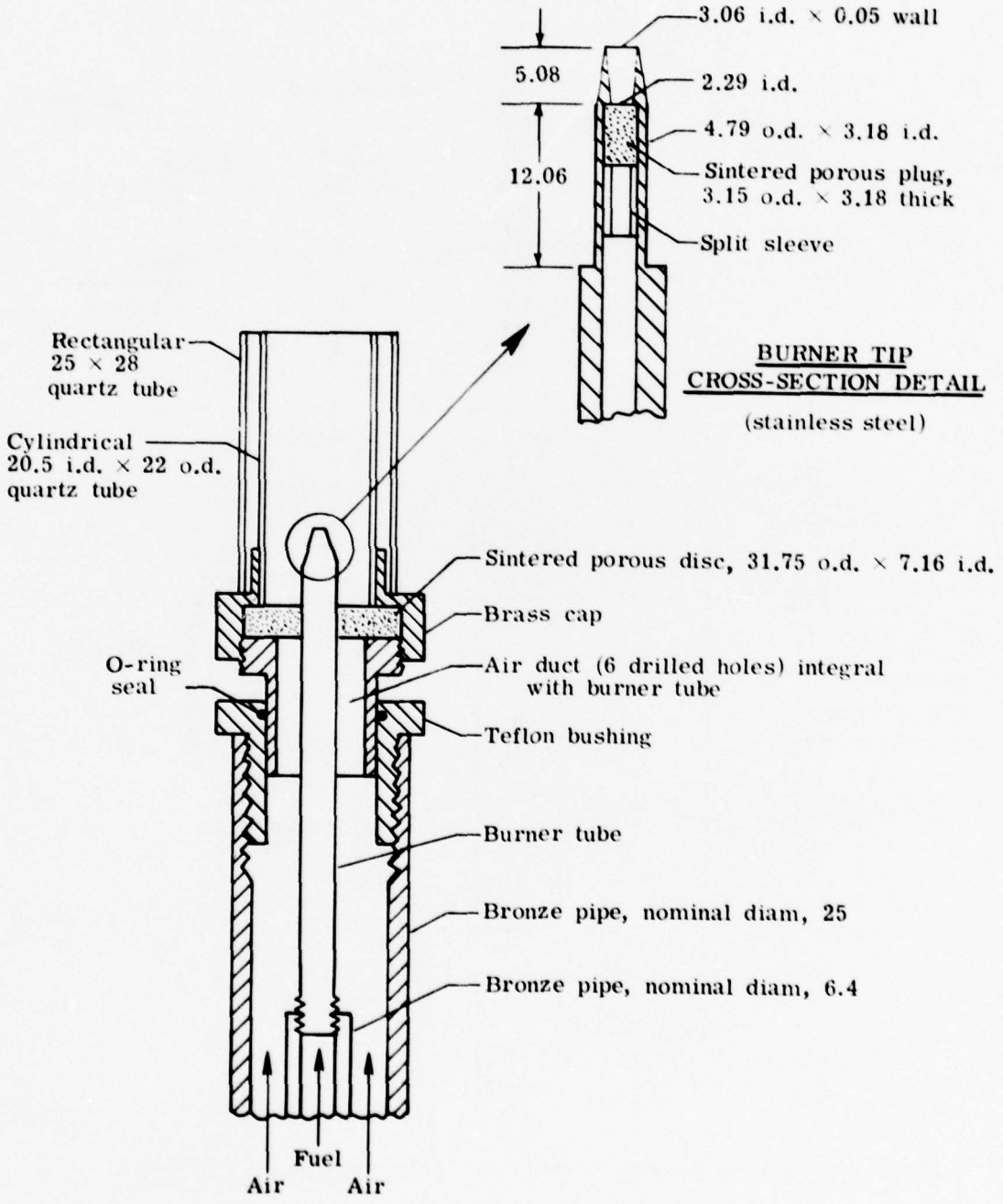


Figure 1.- Burner assembly and detail. All dimensions are in millimeters.

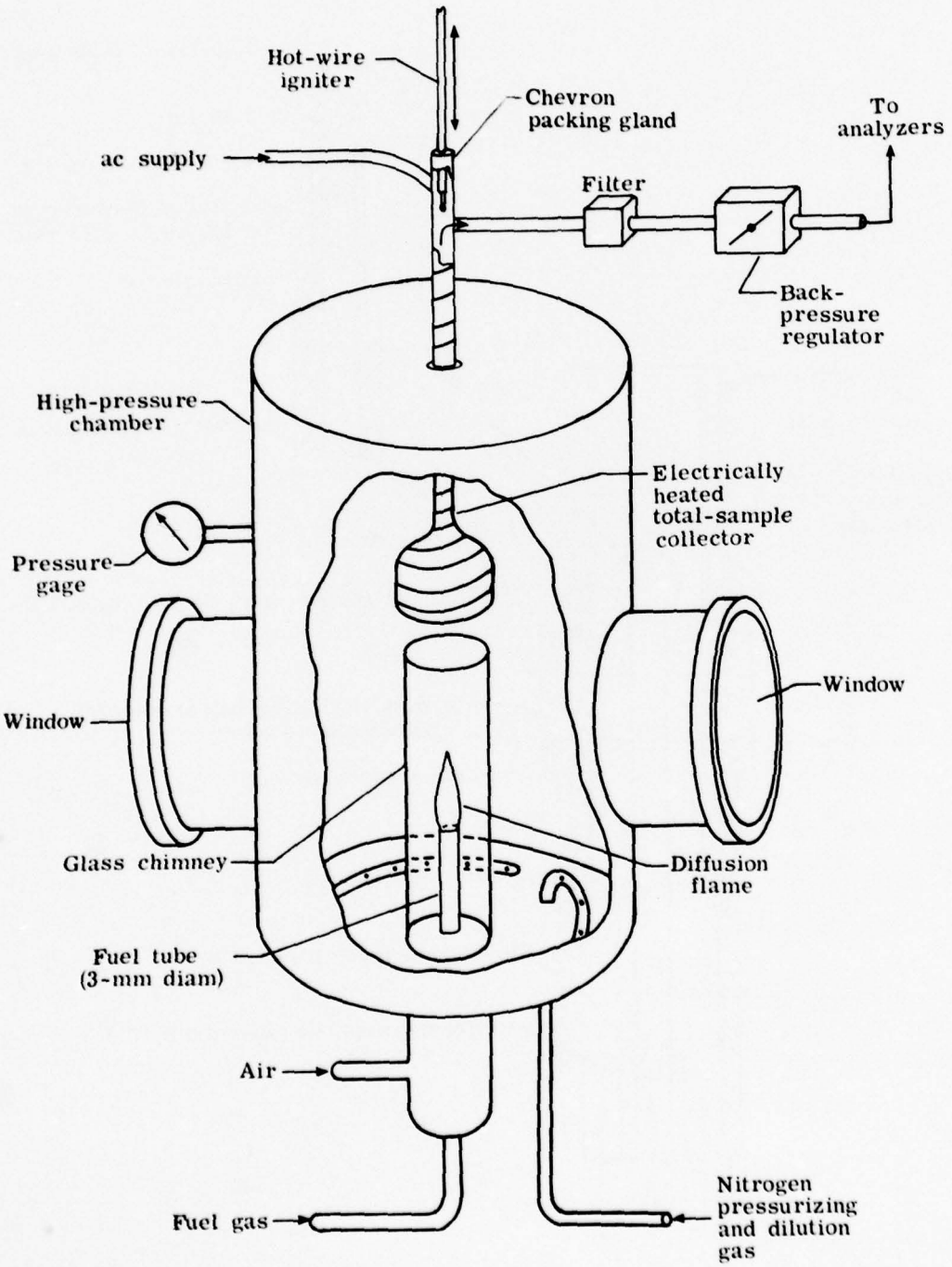


Figure 2.- Schematic diagram of burner and sample collection system.

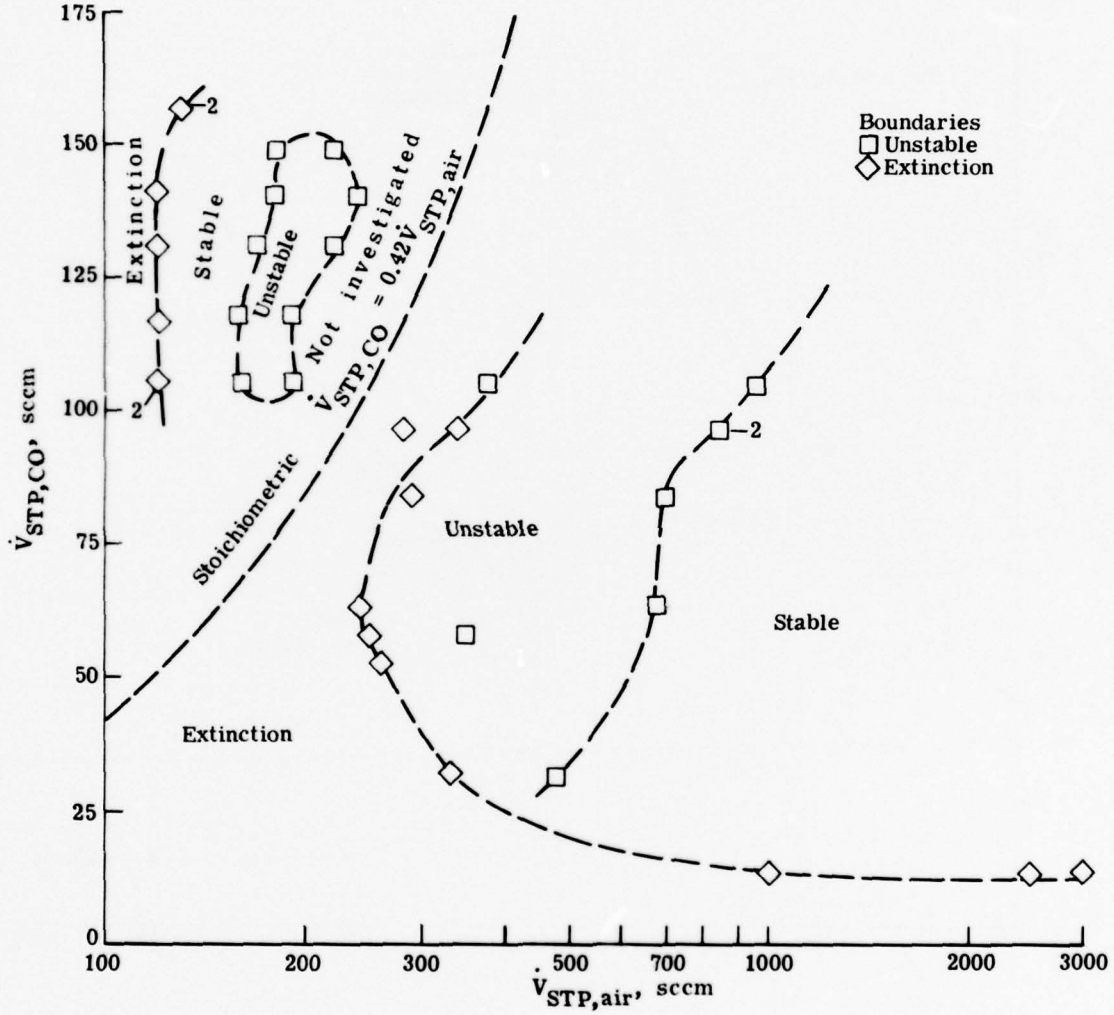


(a) p = 1 atm.

Figure 3.- Stability and extinction limits.

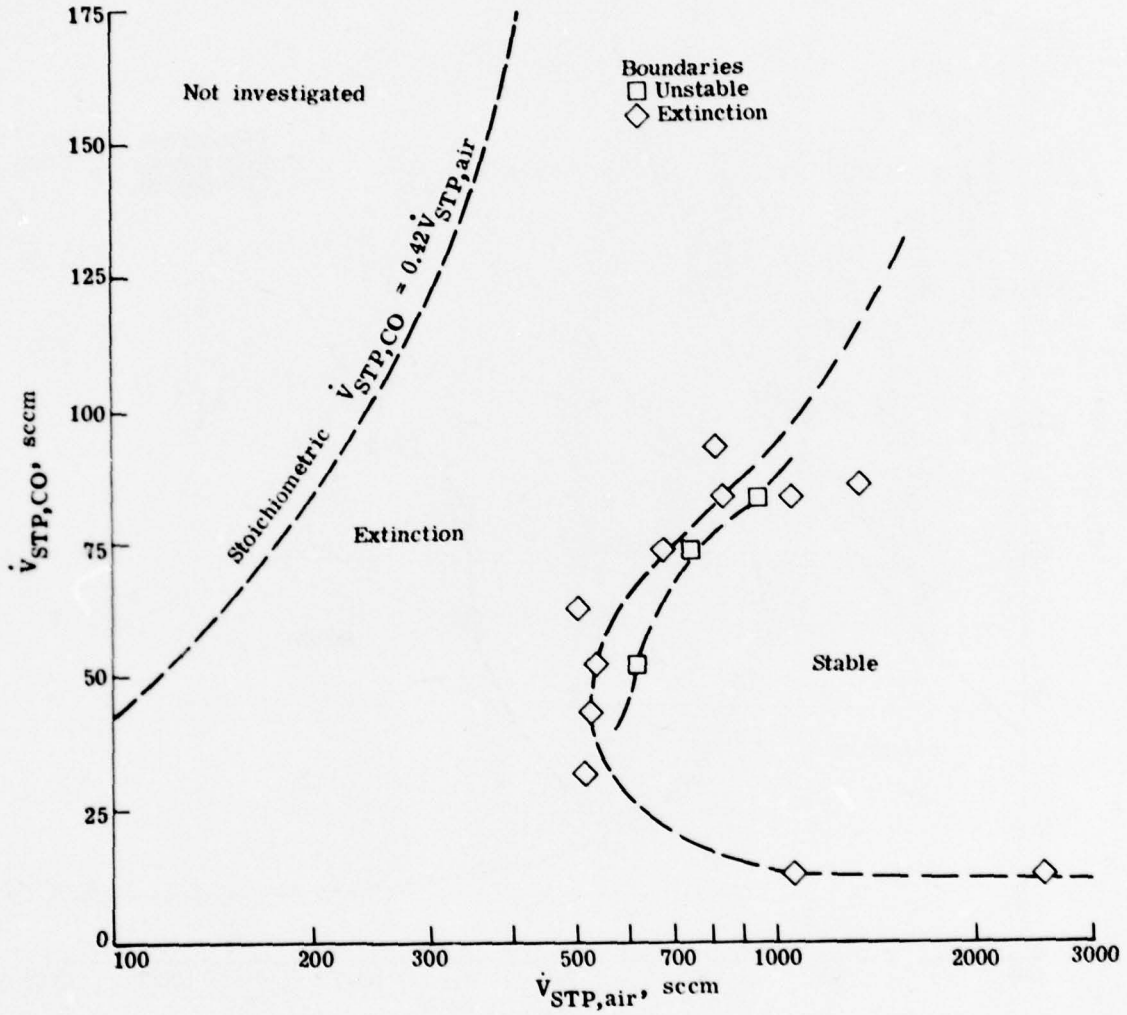


(b) p = 20 atm.

Figure 3.- Continued.

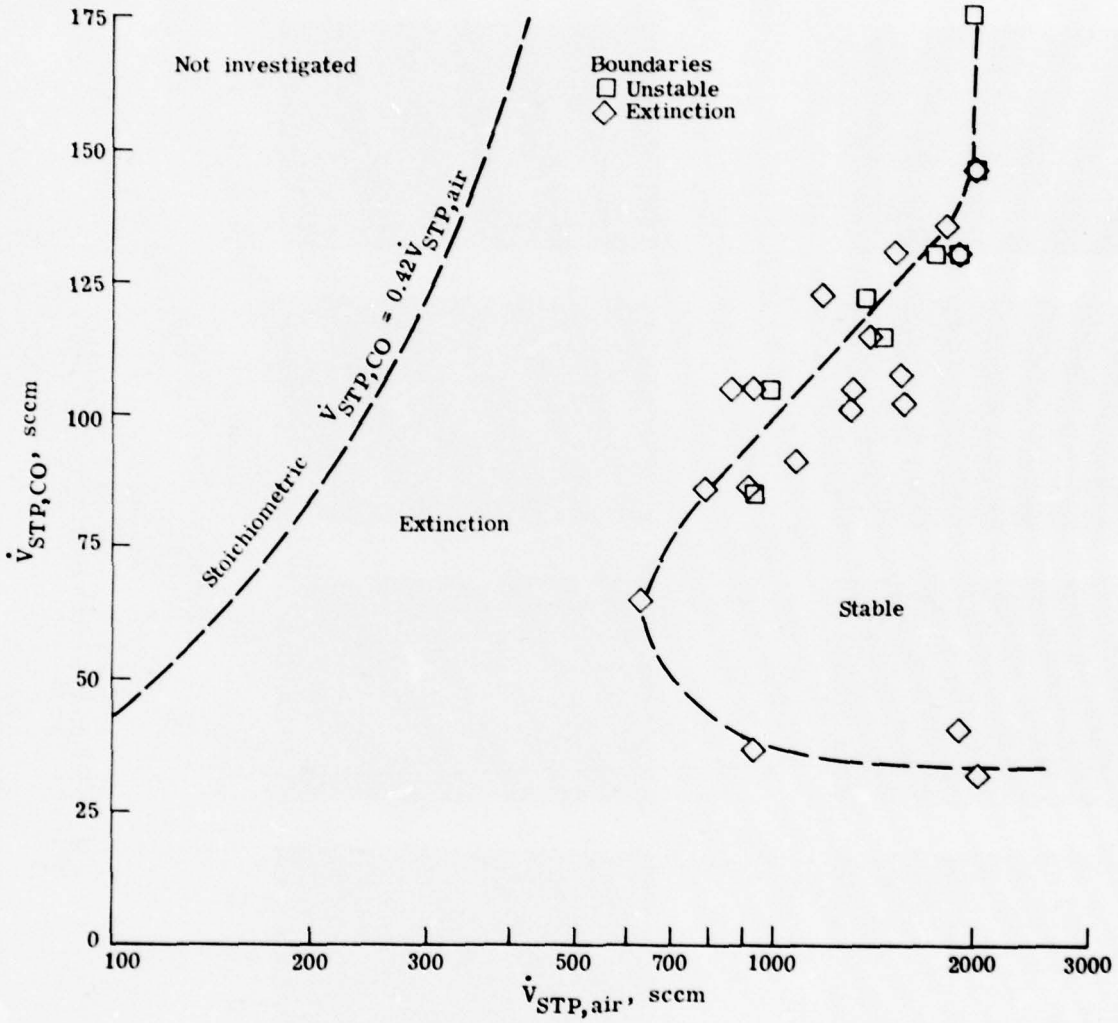


(c) p = 50 atm.

Figure 3.- Concluded.

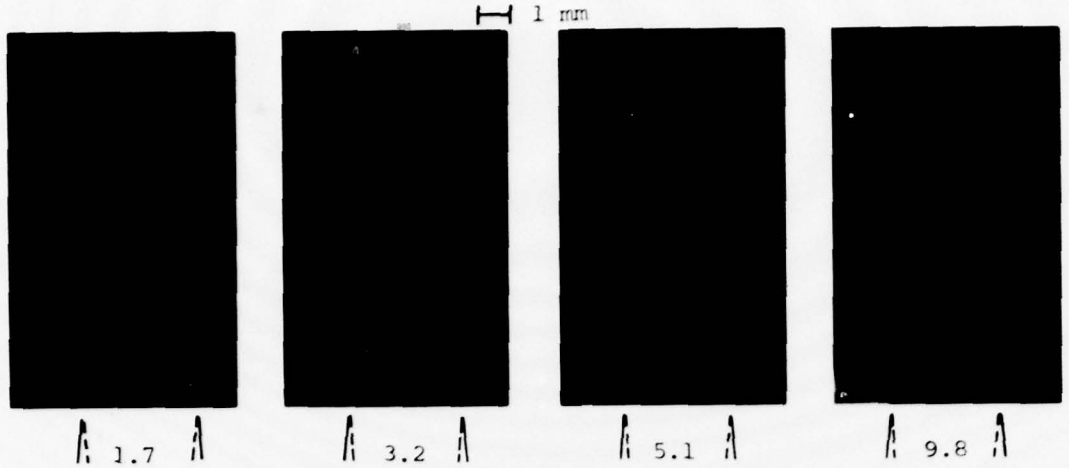


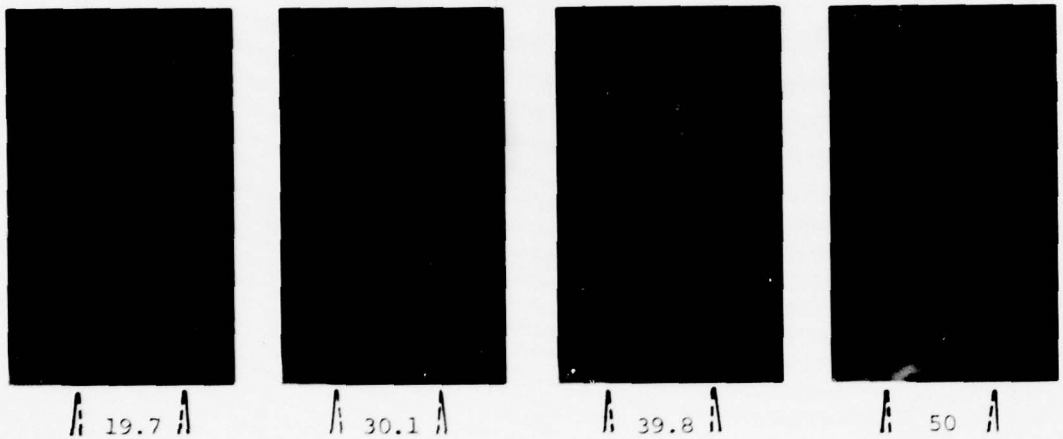


L-79-274

(a) 73-sccm CO.

Figure 4.- Photographs of flame.

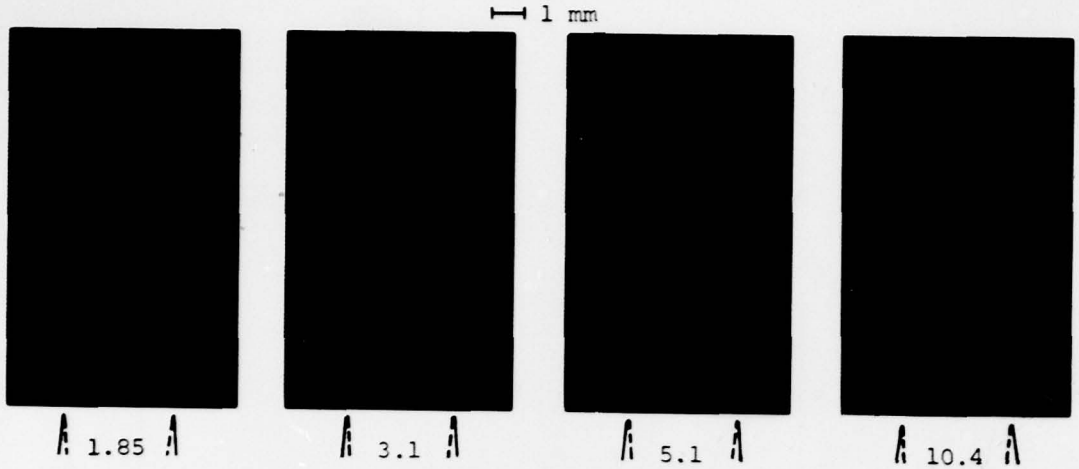


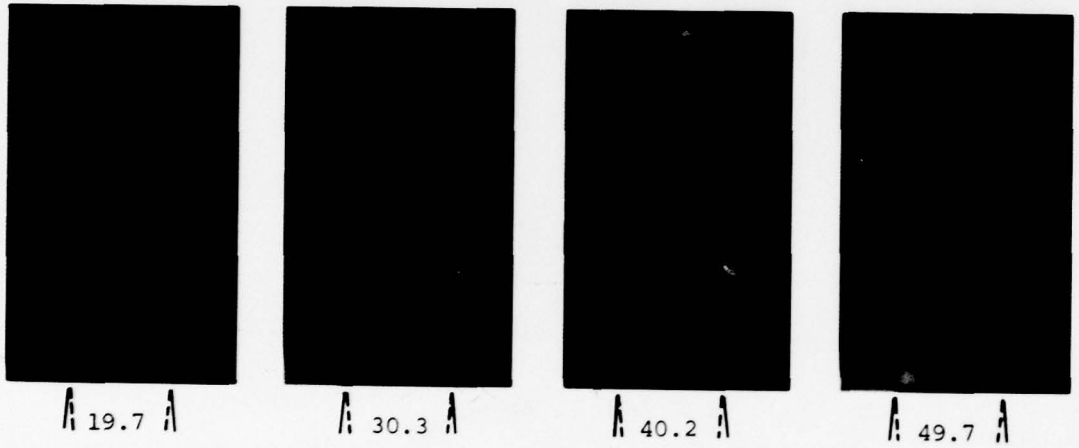


L-79-275

(b) 146-sccm CO.

Figure 4.- Concluded.

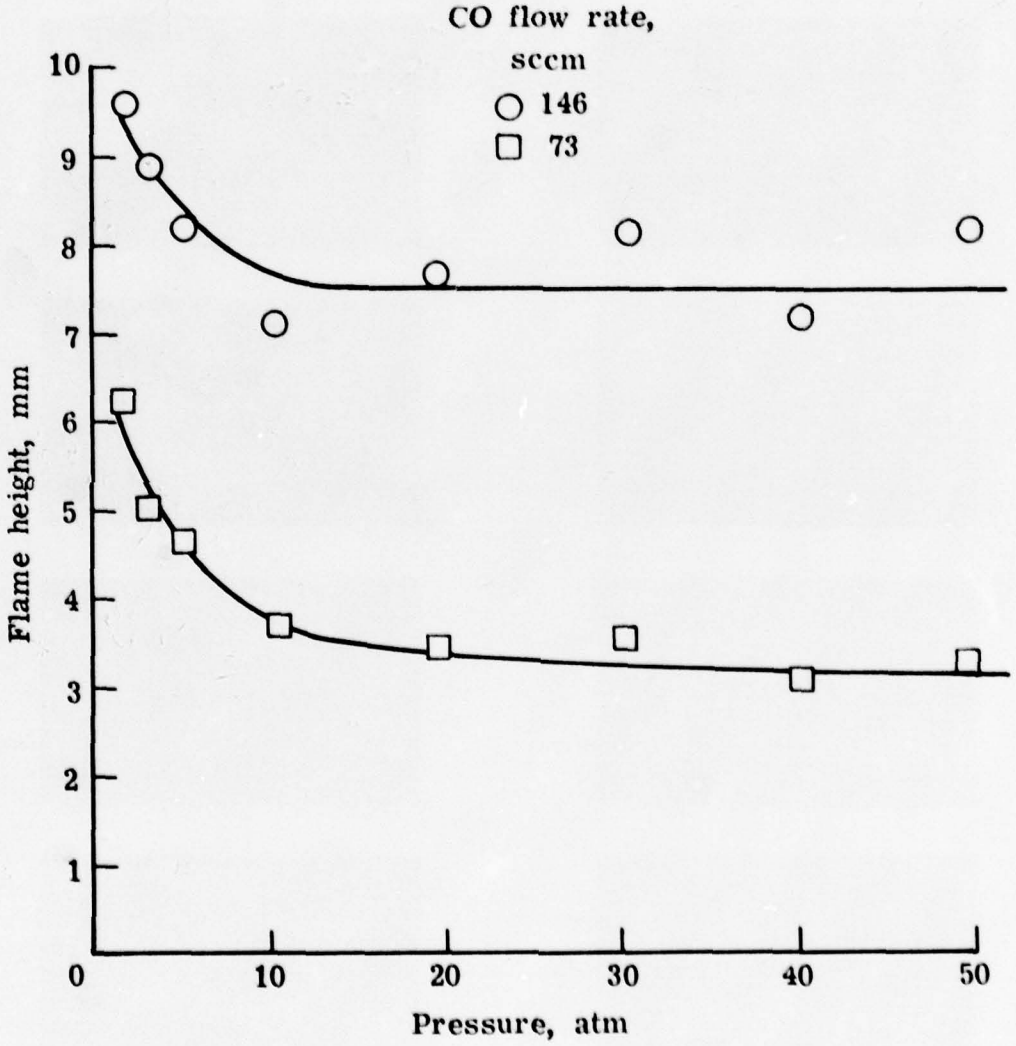


Figure 5.- Flame height as function of pressure.

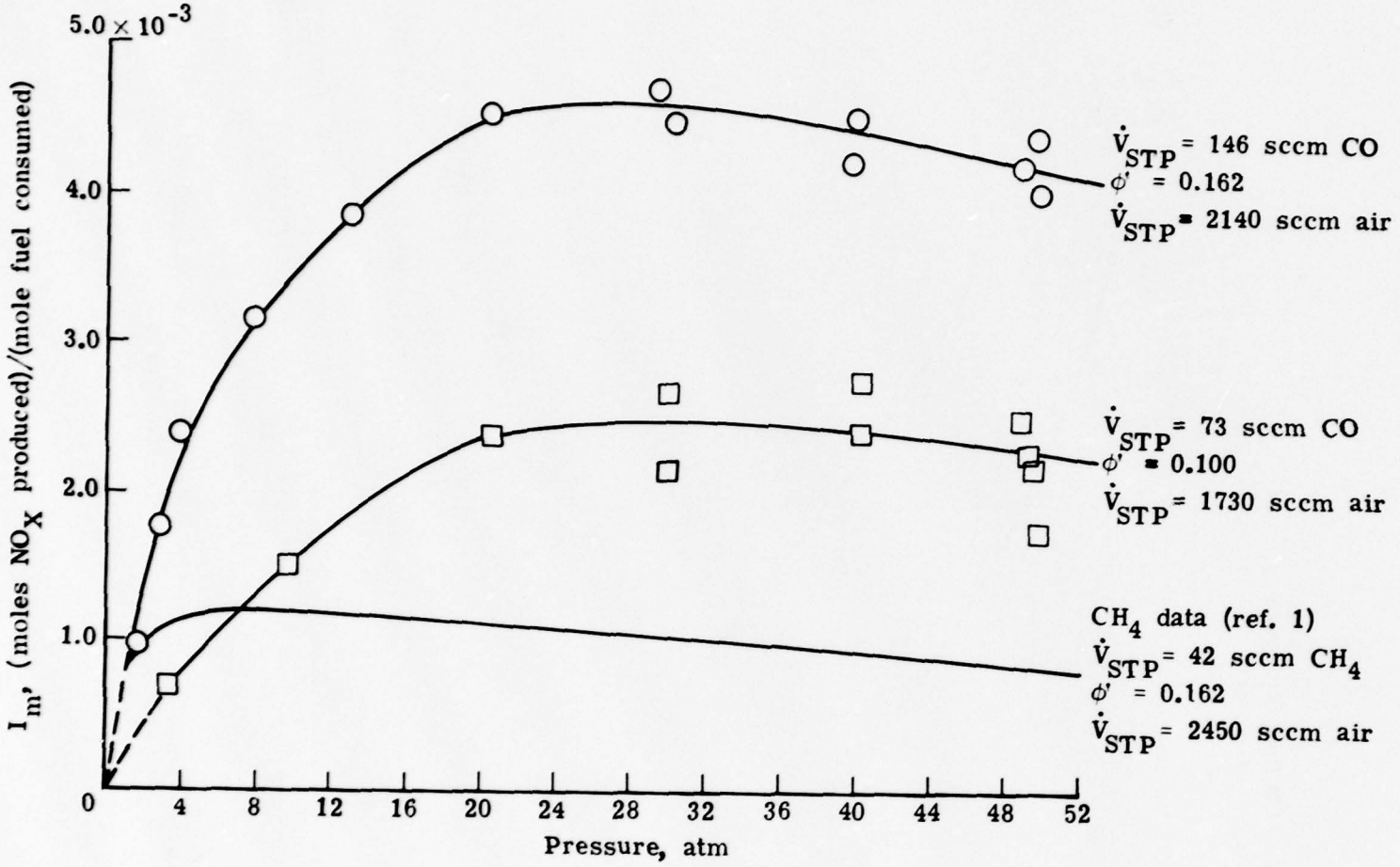


Figure 6.- Molar emission index plotted against pressure for CO-air diffusion flames.

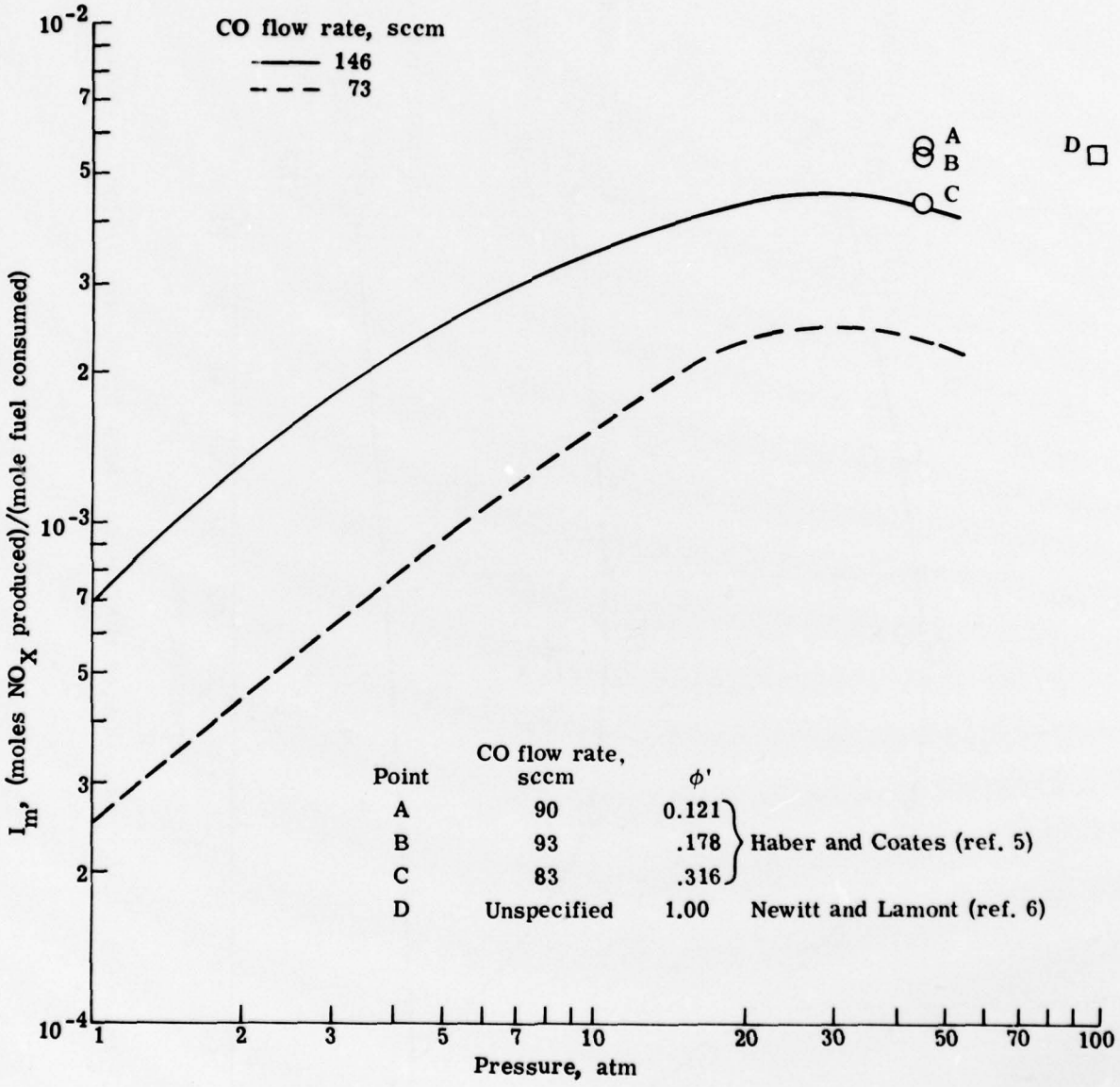


Figure 7.- Molar emission index plotted against pressure for CO-air diffusion flames.

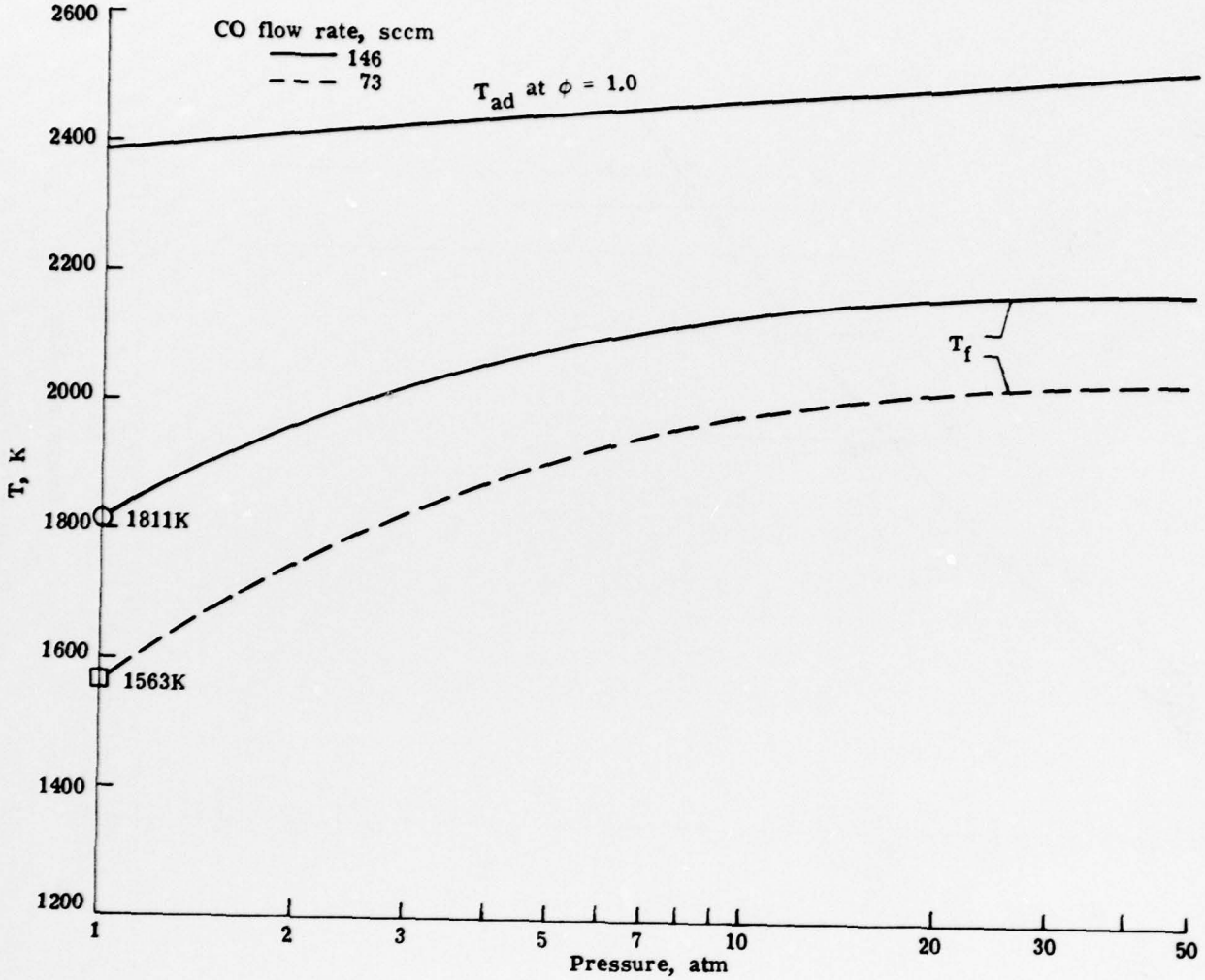


Figure 8.- Temperature as function of pressure.

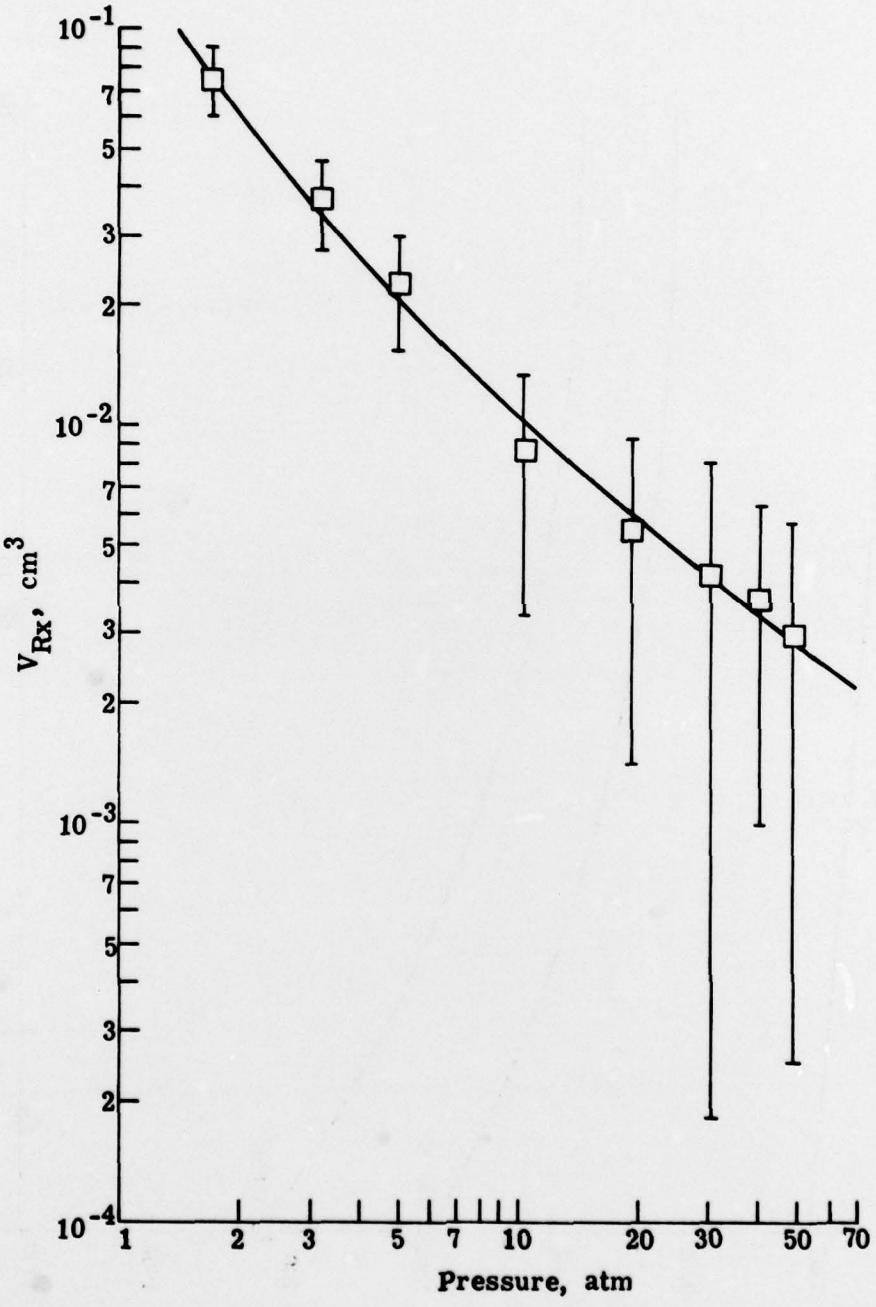


(a) 73-sccm CO flame.

Figure 9.- Reaction volume. Bars indicate estimated error boundaries.

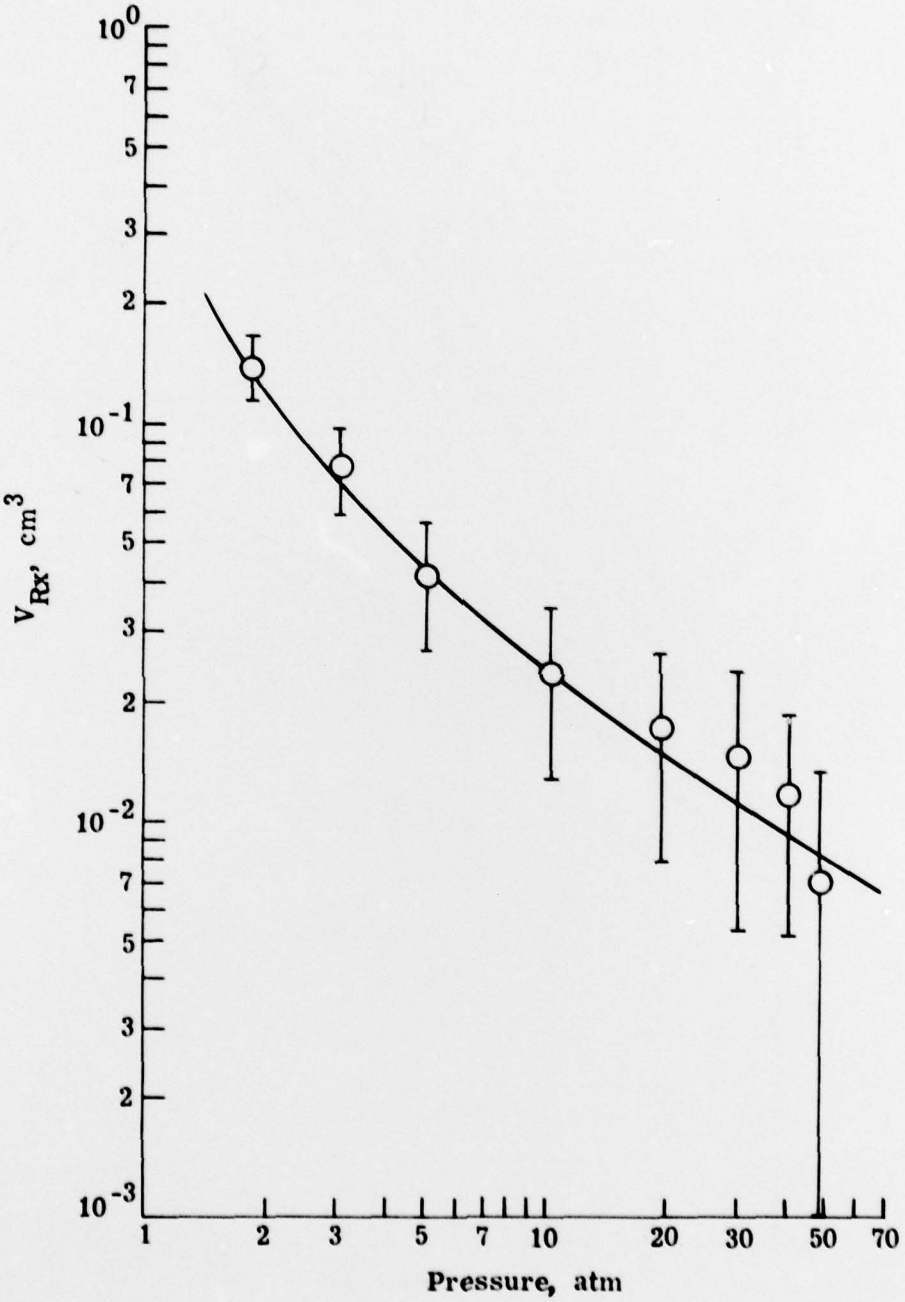


(b) 146-sccm CO flame.

Figure 9.- Concluded.

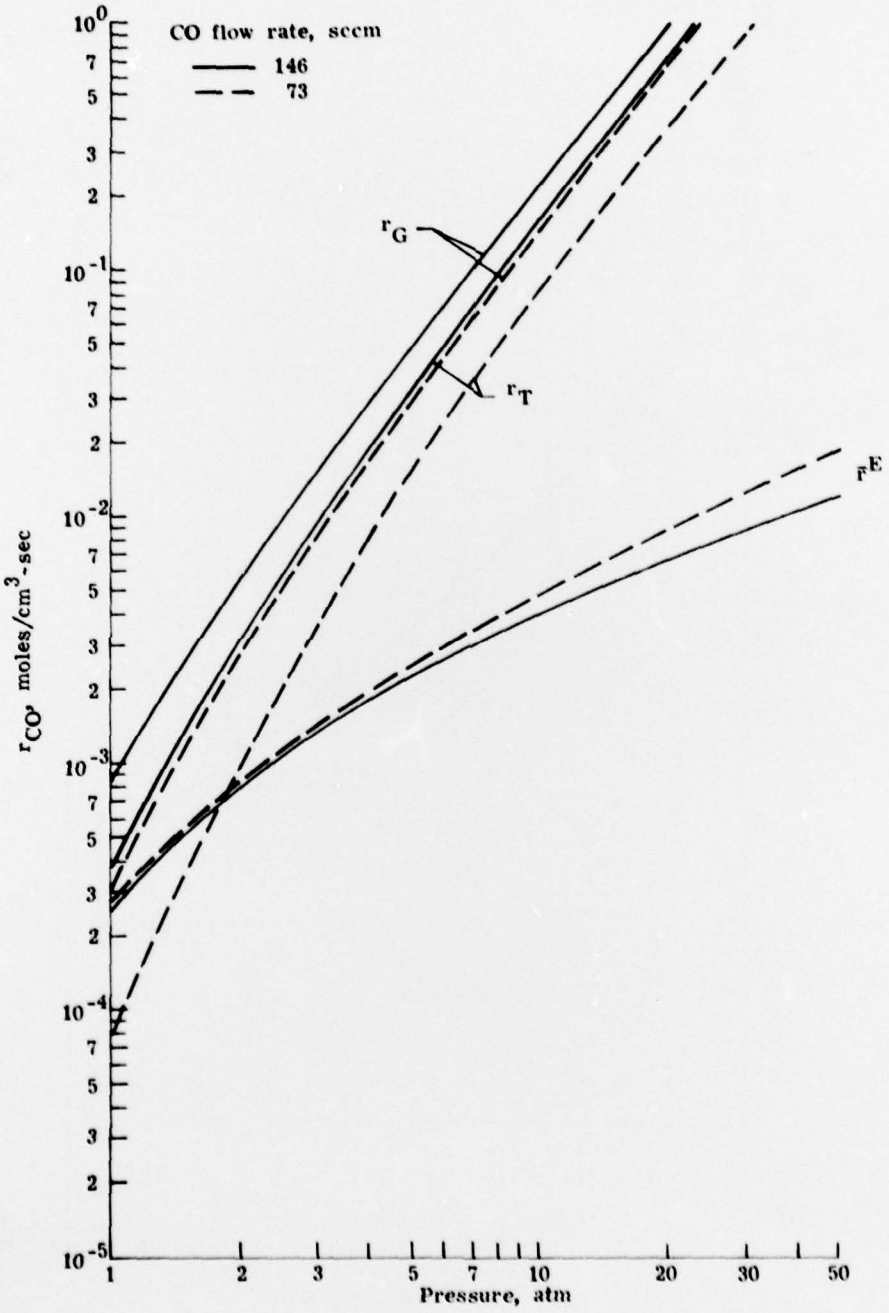


(a) Reaction rate.

Figure 10.- Reaction and diffusion rate of CO.

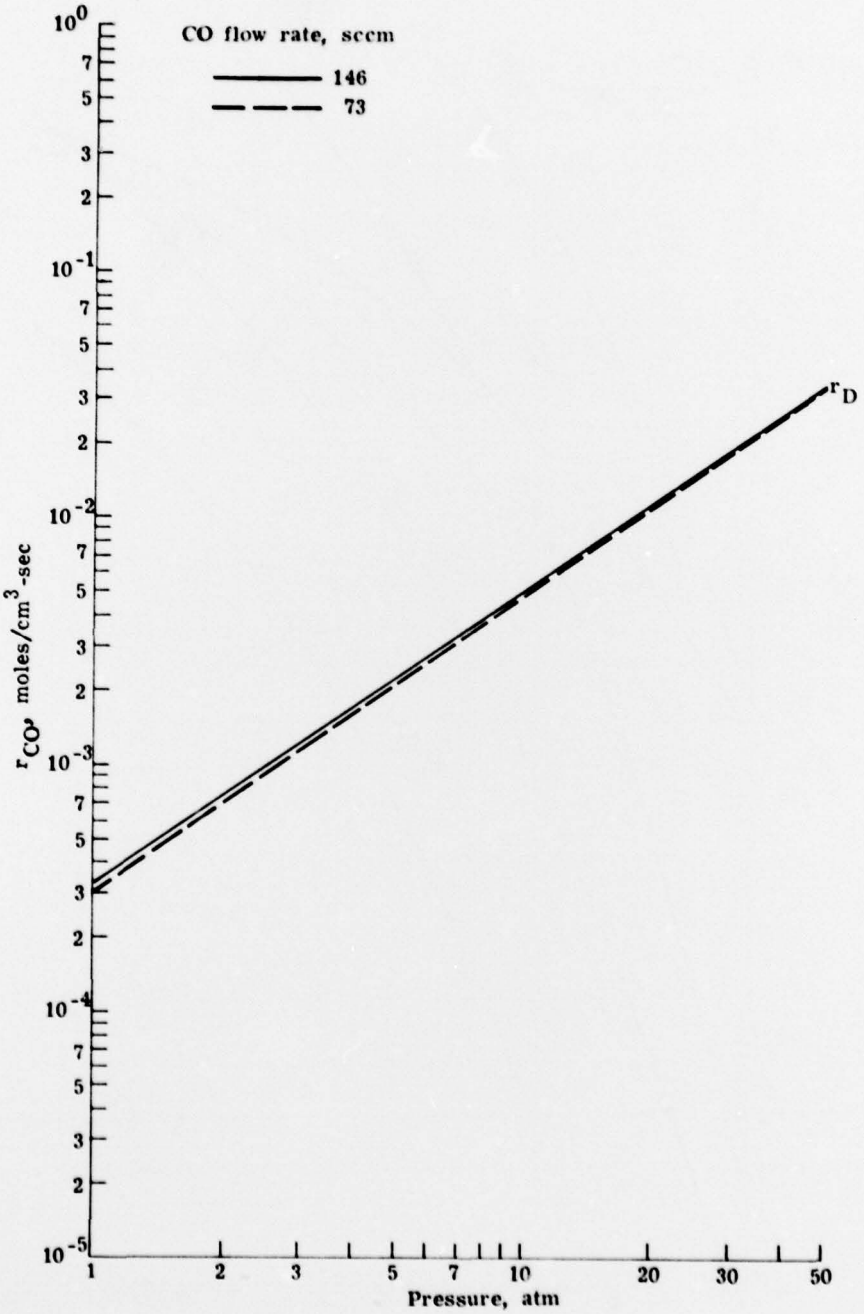


(b) Diffusional rate into flame zone.

Figure 10.- Concluded.

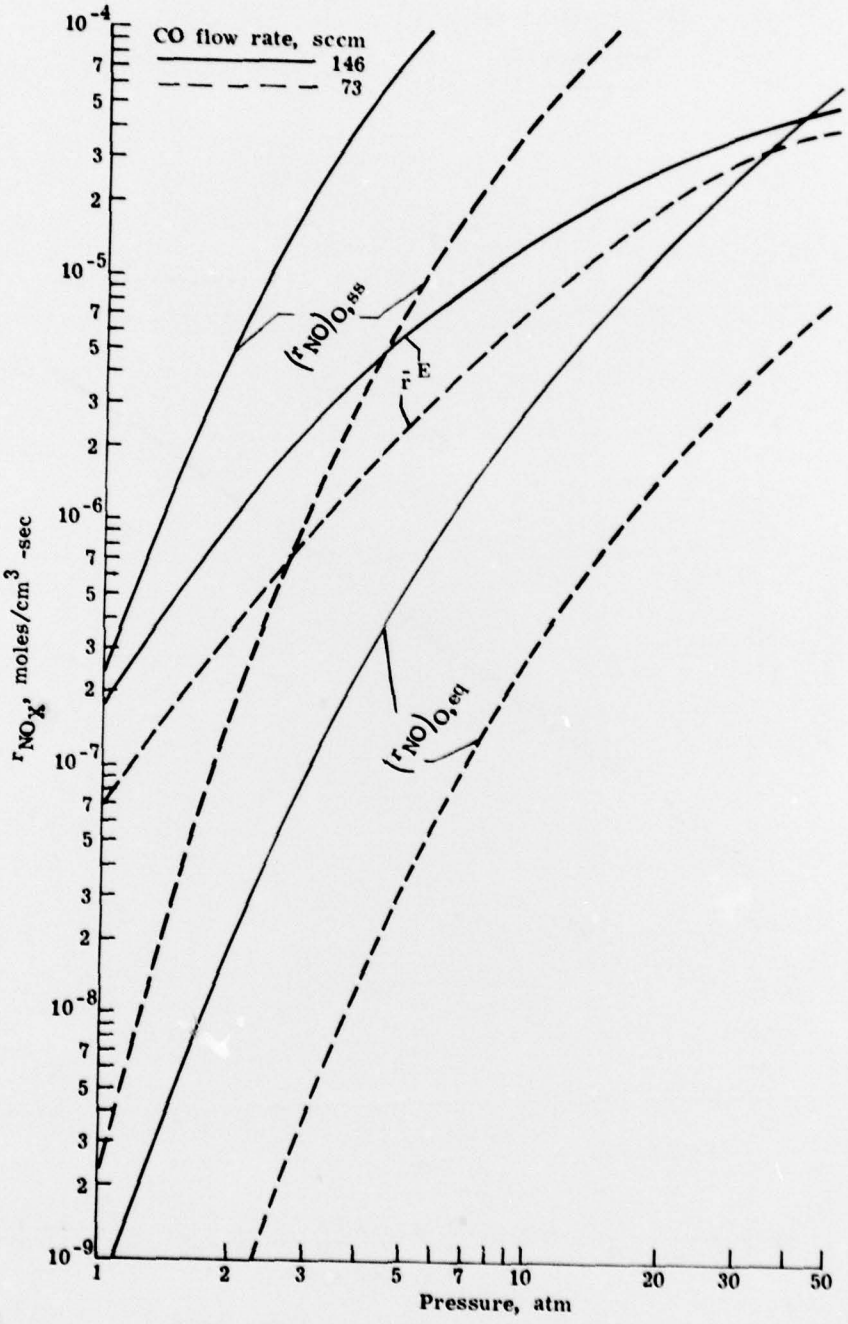


Figure 11.- Formation rate of $NO_X$.

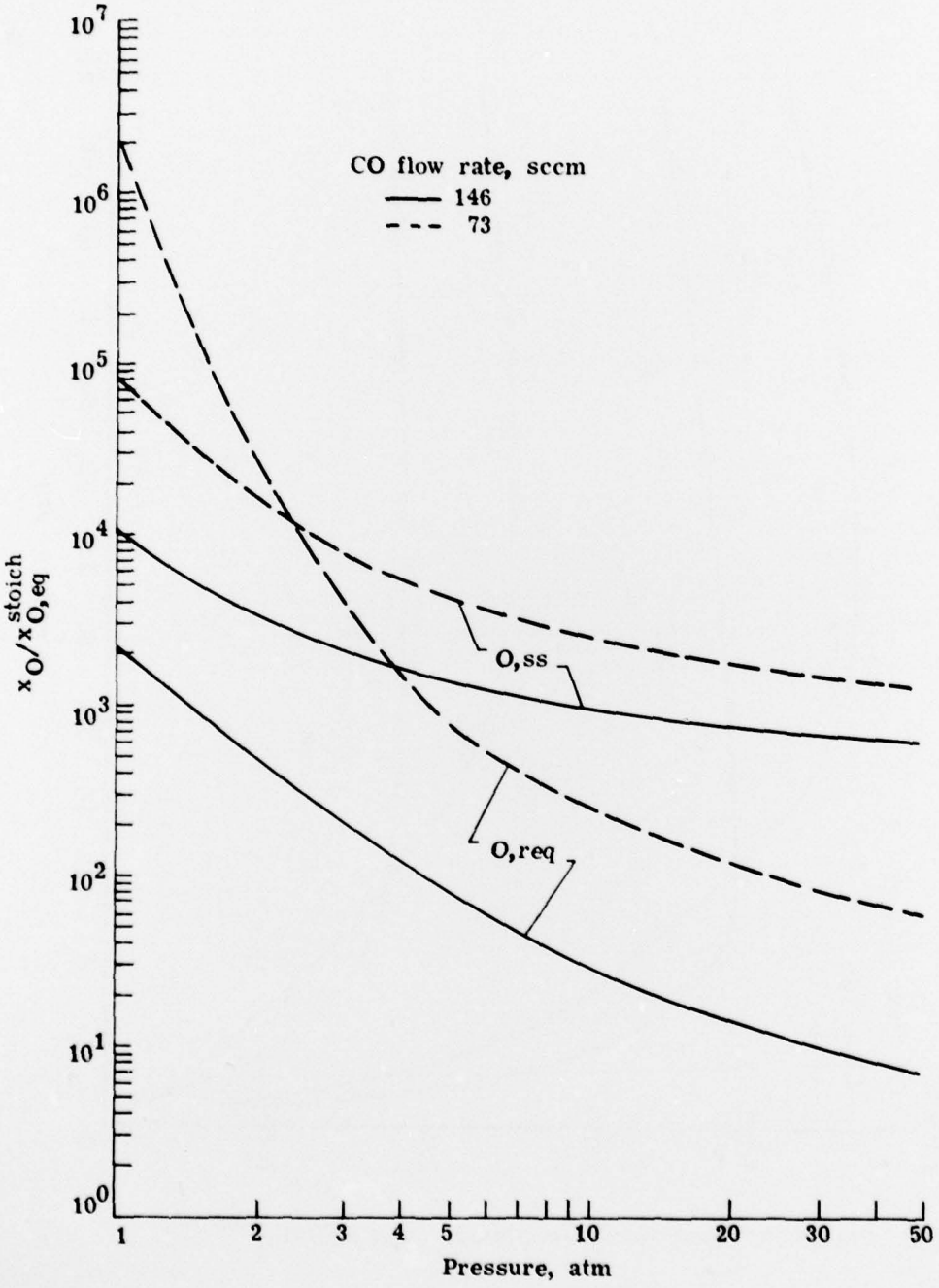


Figure 12.- Superequilibrium oxygen-atom ratio.

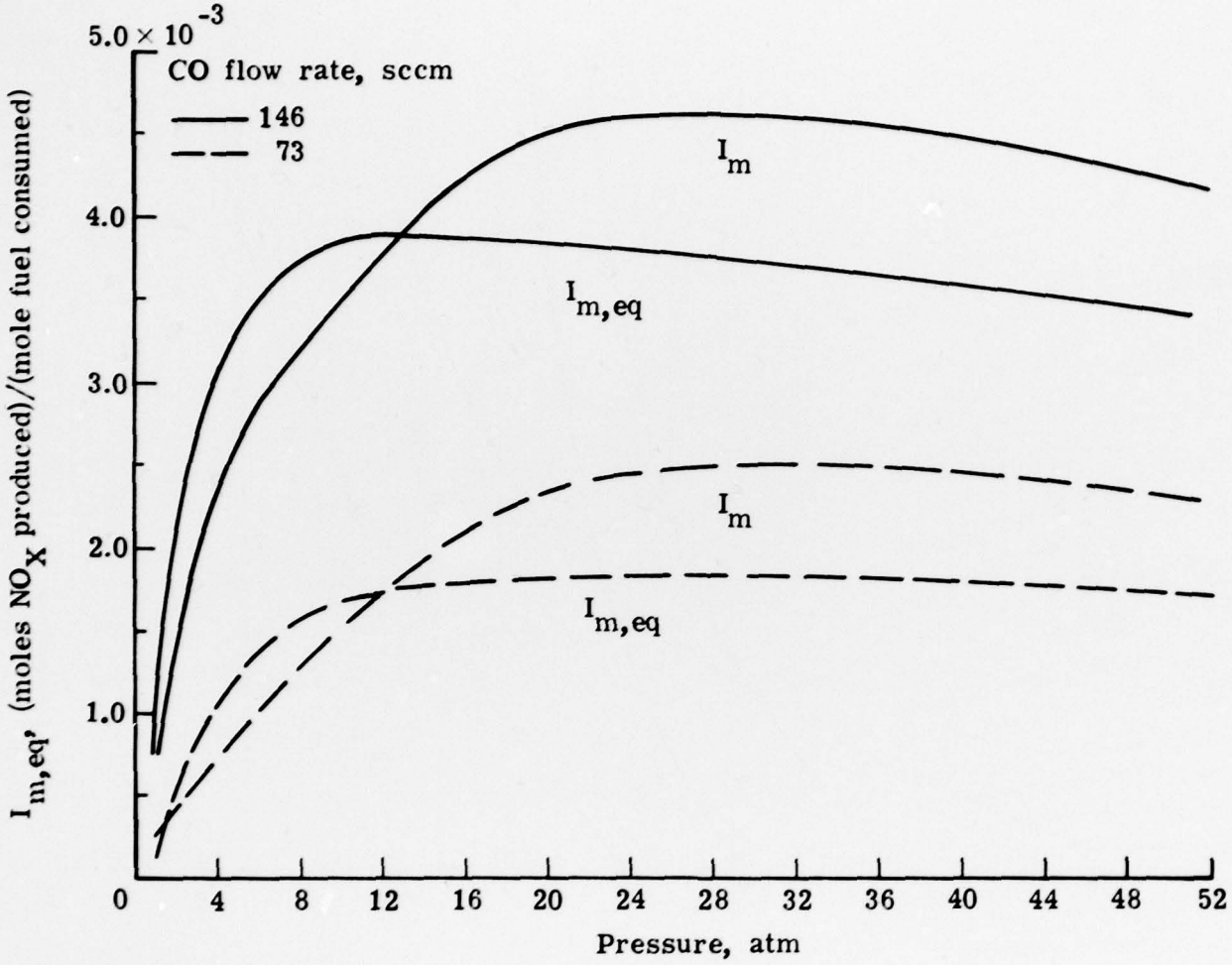


Figure 13.- Equilibrium molar emission index at $T = T_f$ and $\phi = 1$.

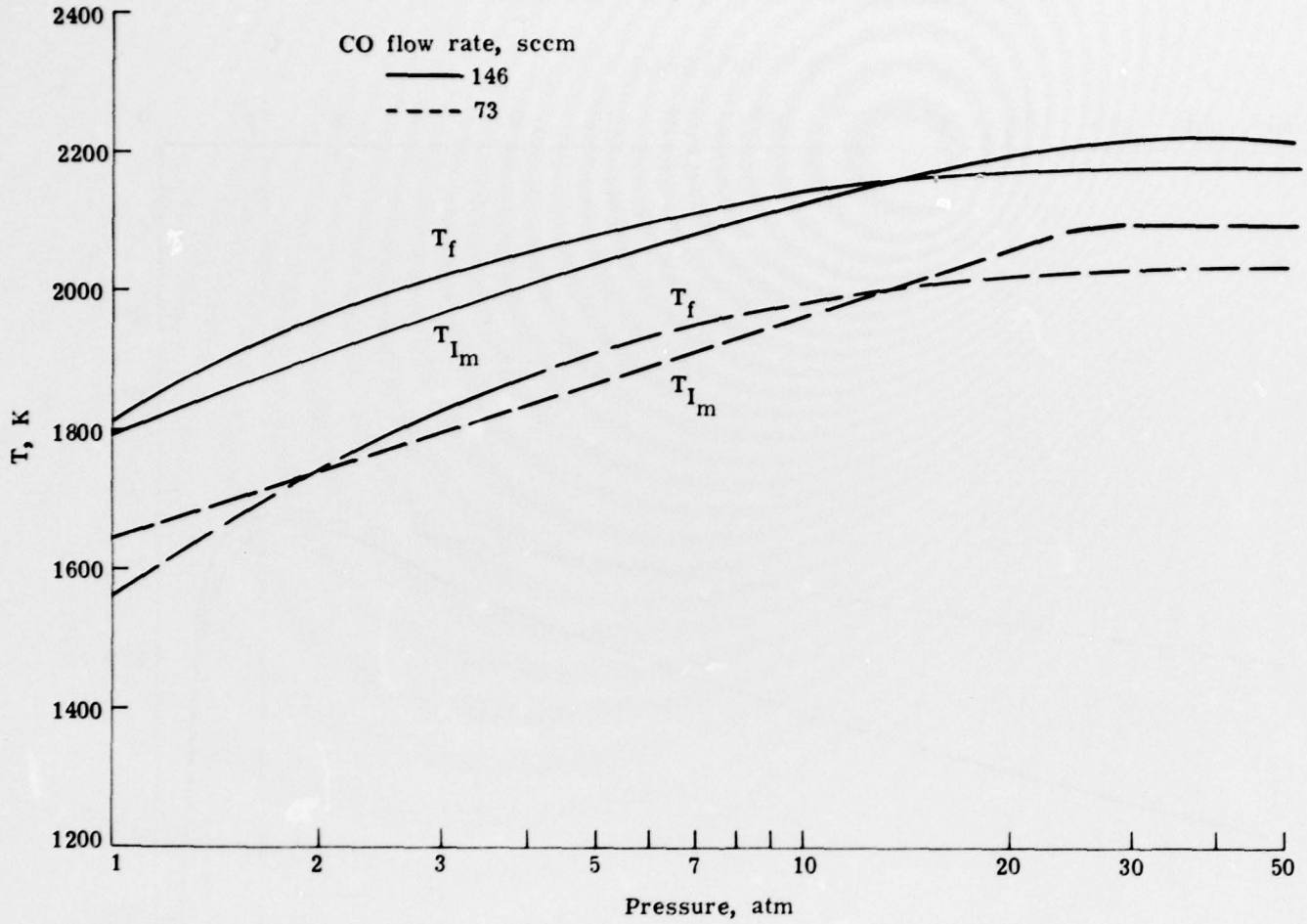


Figure 14.- Required temperature for equilibrium molar emission index to equal experimentally observed molar emission index.

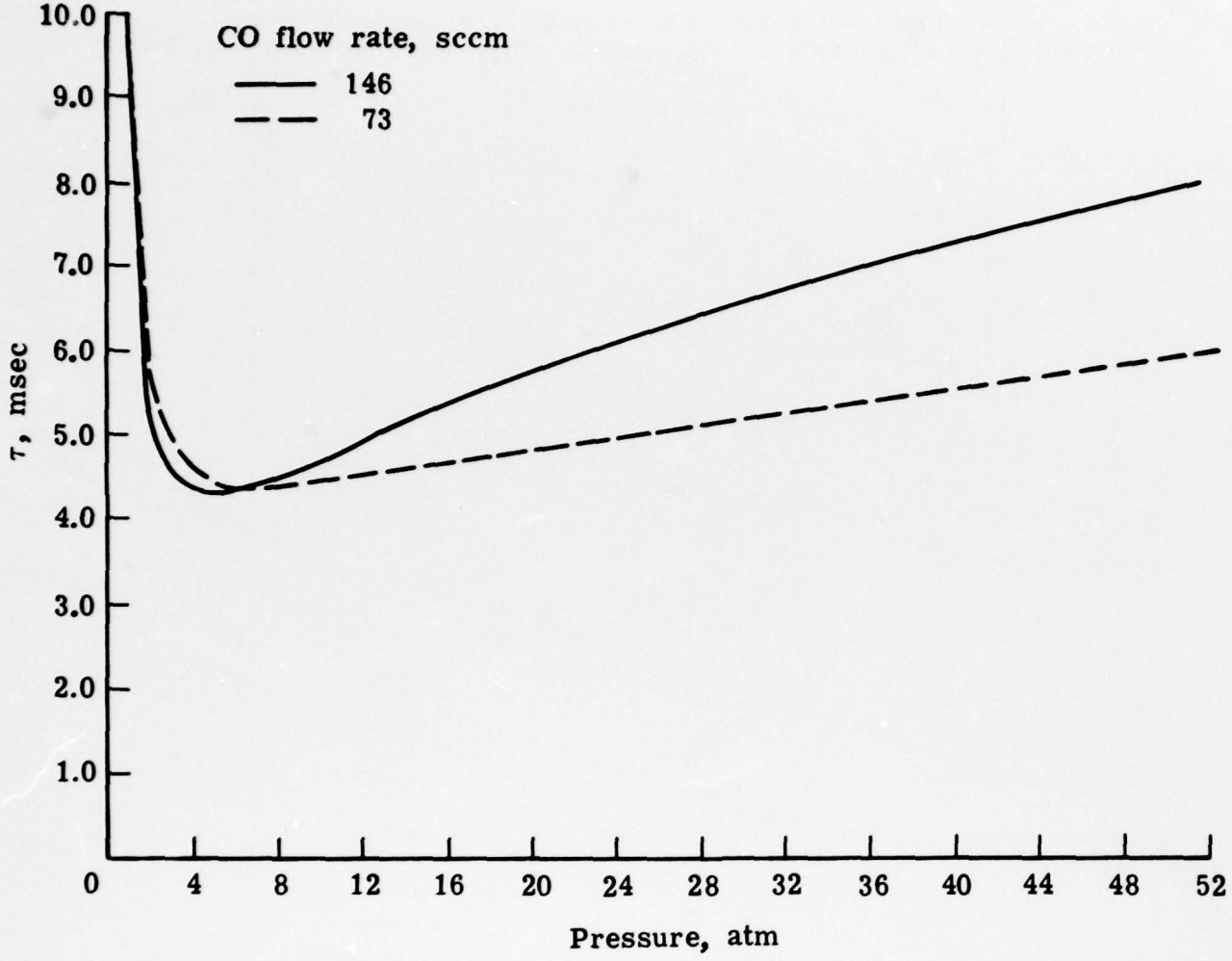


Figure 15.- Residence time as function of pressure.

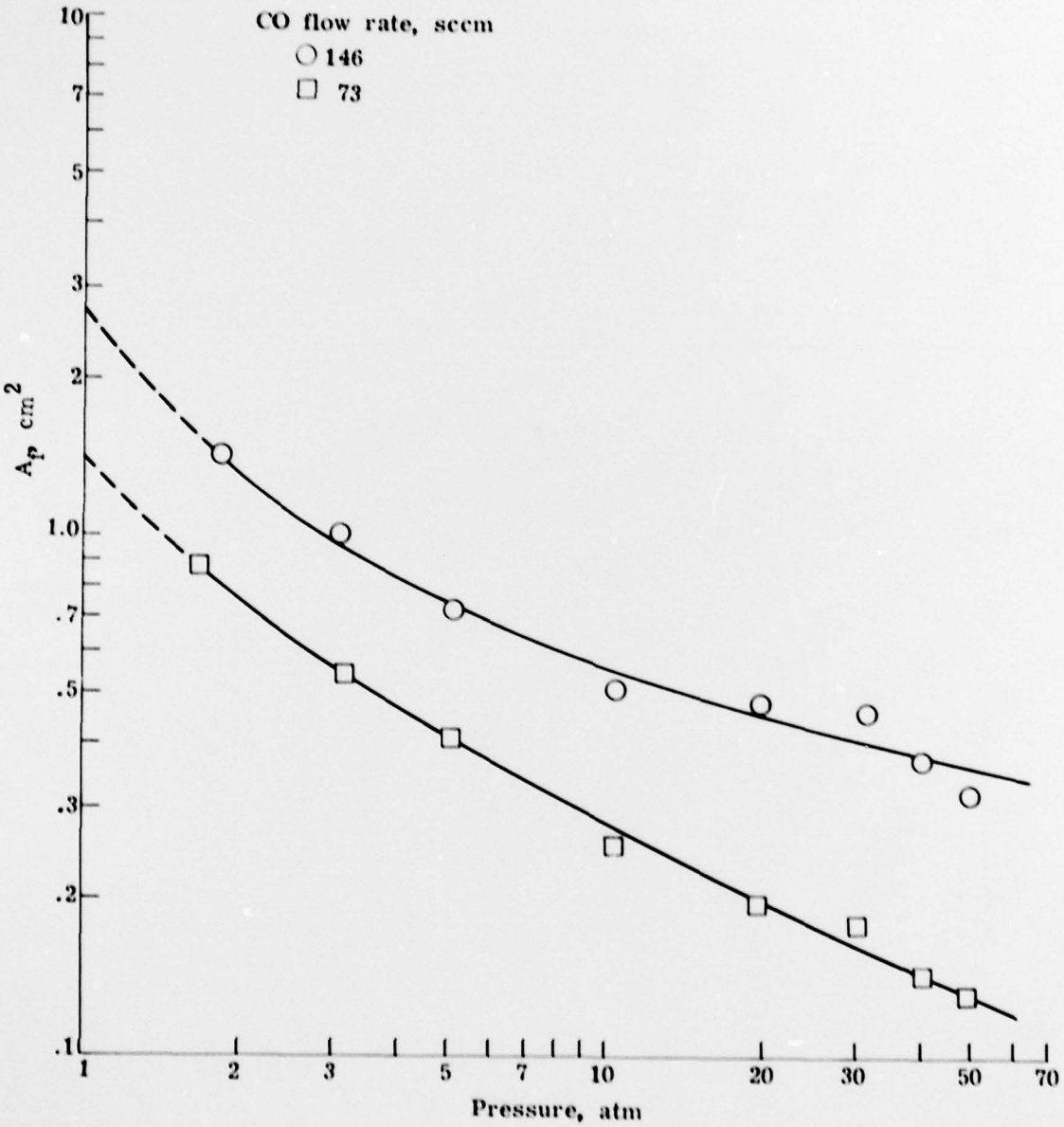


Figure 16.- Surface area of flame.

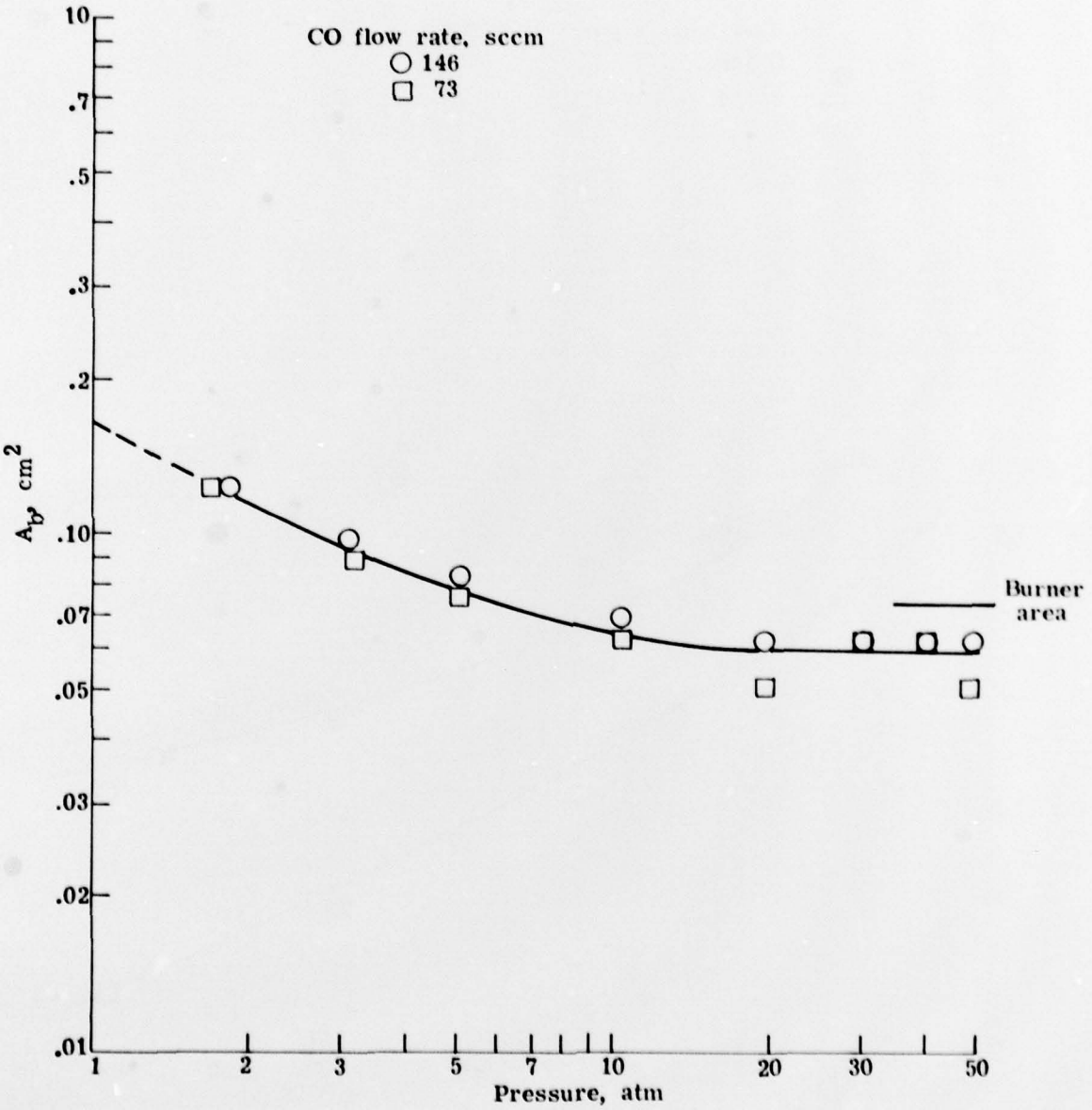


Figure 17.- Projected area of base of flame.

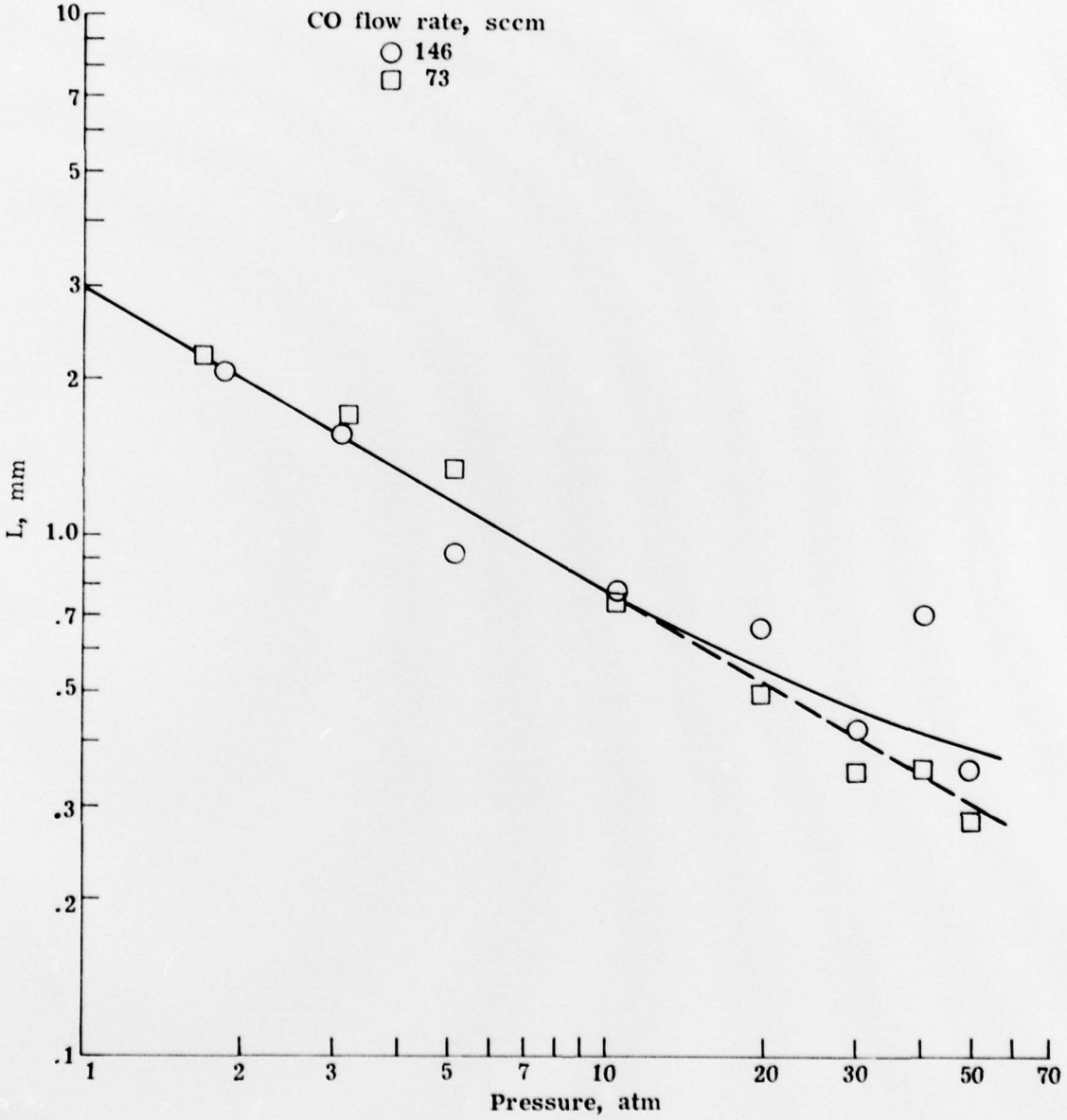


Figure 18.- Flame thickness path length.

(18) NASA (19) TP-1448

| 1. Report No. | 2. Government Accession No. | 3. Recipient's Catalog No. |
|---|---|---|
| NASA TP-1448 | | |

| 4. Title and Subtitle | 5. Report Date |
|---|---|
| EFFECT OF PRESSURE ON STRUCTURE AND $NO_x$ FORMATION IN CO-AIR DIFFUSION FLAMES | October 1979 |
| | 6. Performing Organization Code |
| 7. Author(s) | 8. Performing Organization Report No. |
| Howard G. Maahs and Irvin M. Miller | L-12731 |
| | 10. Work Unit No. 505-03-23-01 |
| 9. Performing Organization Name and Address | 11. Contract or Grant No. |
| NASA Langley Research Center<br>Hampton, VA 23665 | |
| 12. Sponsoring Agency Name and Address | 13. Type of Report and Period Covered |
| National Aeronautics and Space Administration<br>Washington, DC 20546 | Technical Paper |
| | 14. Sponsoring Agency Code |

15. Supplementary Notes

16. Abstract

A study has been made of flame structure and nitric oxide formation in confined laminar CO-air diffusion flames over a pressure range from 1 to 50 atm. The shape of the flames changed from wide and convex at 1 atm to slender and concave at 50 atm, with the greatest change occurring below about 10 atm. Flame height decreased with increasing pressure from 1 atm to about 10 atm, but was independent of pressure at higher pressures. The regimes of stable burning decreased with increasing pressure up to 50 atm, with the greatest reduction occurring between 1 atm and 20 atm.

The molar emission index (the moles of nitrogen oxides formed per mole of carbon monoxide consumed) increased as the pressure was increased above 1 atm, reached a maximum at approximately 28 to 30 atm, and thereafter decreased slowly up to 50 atm. Circumstantial evidence is offered to support the proposition that the concentrations of nitrogen oxides in the flames approach their equilibrium values for pressures above about 20 atm.

| 17. Key Words (Suggested by Author(s)) | | 18. Distribution Statement |
|---|---|---|
| Pollution | Emissions | Unclassified - Unlimited |
| Nitric oxide | Combustion | |
| CO-air flame | High pressure | |
| Diffusion flame | | Subject Category 25 |

| 19. Security Classif. (of this report) | 20. Security Classif. (of this page) | 21. No. of Pages | 22. Price* |
|---|---|---|---|
| Unclassified | Unclassified | 55 | $5.25 |

* For sale by the National Technical Information Service, Springfield, Virginia 22161

387 543

JOB